EFFECTS of IONIC COUPLINGS on NUCLEAR ALIGNMENT of Co^{58} in (Zn, Ni)$SiF_6 \cdot 6H_2O$

Thesis by

William Albert Steyert, Jr.

In Partial Fulfillment of the Requirements

for the Degree of

Doctor of Philosophy

California Institute of Technology

Pasadena, California

1960

ACKNOWLEDGMENTS

The author is greatly indebted to Professor John R. Pellam for his profound interest in all phases of this investigation, and for his expert guidance throughout the work. The ease with which these experiments were performed was due chiefly to Professor Pellam's very excellent cryogenic facilities.

To Professors Felix Boehm, Murray Gell-Mann, and John Pellam goes the credit for originating this series of experiments. Valuable discussions with Professor Robert Christy as well as with the above have contributed immeasurably in physically interpreting these results. The theoretical work of Dr. Hans Weidenmuller has been essential to the understanding of the "K-capture effect".

Special thanks go to Professor Jesse W. M. DuMond for his many contributions to this project, and to Mr. John Rogers for his untiring participation in these experiments from their very beginning.

This work was supported by the Alfred P. Sloan Foundation, Inc., the National Science Foundation, and the U. S. Atomic Energy Commission.

ABSTRACT

The γ-rays emitted from traces of Co^{58} aligned in single crystals of $(xNi, (1-x)Zn, Co^{58})SiF_6 \cdot 6H_2O$ have been studied with various nickel fractions (x) between 0 and 0.19.

These experiments were designed to determine the fraction of Fermi decays (λ) in the Co^{58} β-decay. Results using a 0% nickel crystal indicate a small dealignment of the 10^{-11} second intermediate state which just precedes the emission of the 810 kev γ-ray. In addition, the nuclear alignment is found to be strongly influenced by the presence of paramagnetic nickel ions in the nickel bearing crystals. Because of the dealignment in the intermediate state, it is not possible to assign a definite value for λ. However, indications are that λ is near to zero.

TABLE OF CONTENTS

TABLE OF CONTENTS (cont.)

TABLE OF CONTENTS (cont.)

FIGURES

FIGURES (cont.)

TABLES

INTRODUCTION

In 1926 Debye (Ref. 1) and Giauque (Ref. 2) independently proposed a method of obtaining temperatures less than $1^{\circ}K$. This was by the adiabatic demagnetization of a paramagnetic crystal. The first experimental results were obtained in 1933 and 1934 by DeHaas and Wiersma (Ref. 3) in Leiden, by Giauque and McDougall (Ref. 4) in Berkeley, and by Kurti and Simon (Ref. 5) in Oxford.

With as low as $0.001^{\circ}K$ available it was now possible to polarize nuclei by means of their very small interaction with a magnetic or electric environment. The following methods of stationary alignment were proposed:

1. Polarization of nuclei on external magnetic field (Ref. 6 and 7).
2. Polarization of paramagnetic electrons by an external magnetic field. The electrons in turn polarizing the nuclei by hyperfine interactions (Ref. 8 and 9).
3. Alignment of paramagnetic electrons by a crystalline field, followed by nuclear alignment by hfs (Ref. 10).
4. Alignment of paramagnetic electrons by an anti-ferromagnetic or ferromagnetic interaction. Nuclear alignment by hfs (Ref. 11,12,13,14).

5. Alignment by the interactions of the nuclear electric quadrupole with a local field gradient produced by asymmetrical electron clouds (Ref.15).

More recently non-stationary methods have been proposed to achieve nuclear alignment. Some form of "pumping" mechanism such as a magnetic field, light, rf, etc., puts the nuclei in a non-equilibrium distribution. These methods generally rely on hfs; however the alignment is maintained only for times the order of spin-spin and/or spin-lattice relaxation times. While these non-stationary methods shed light on some very interesting solid state problems, they are not very precise as a nuclear tool because the alignment cannot be predicted by thermodynamics--a dynamic non-equilibrium situation is involved. A brief review of the theoretical and experimental work in all these alignment areas appears in Gorter's "Progress in Low Temperature Physics" (Ref. 16).

By studying the angular distribution of particles emitted by aligned radioactive nuclei we can obtain nuclear information. Many such studies had been completed at the time the experiments to be described were initiated. In particular, Griffing and Wheatley (Ref. 17) had aligned Co^{58} in (0.23 Cu, 0.77 Zn)$K_2(SO_4)_2 \cdot 6H_2O$. They obtained a measurement of nuclear parameter "λ" which measures the fraction of Fermi β-decays in the 470 kev position emission of Co^{58}. They measured the angular distribution of the 810 kev γ-ray following this

β-decay (Fig. 1). Their value of 0.11 ± 0.04 for λ was in conflict with the value of $\lambda < 0.012$ obtained by Boehm and Wapstra (Ref. 19) by applying the theory of β-decay (Ref. 20) to their β-γ circular polarization measurements.

In an effort to resolve this discrepancy Co^{58} was aligned in $Ce_2(Co^{58}, Mg)_3(NO_3)_{12}\cdot 24H_2O$ (Appendix XII). However, results of these experiments were inconclusive because of the presence of two non-equivalent cobalt lattice sites in the crystal--the relative populations of the two sites being unknown (Ref. 21).

For this reason, investigations were carried out using the much more favorable salt, $(Ni, Zn)SiF_6\cdot 6H_2O$. The equivalent spin Hamiltonian describing the energy levels and eigenstates for traces of Co^{59} in $ZnSiF_6\cdot 6H_2O$ is well known from paramagnetic resonance work. There is only one lattice site (exclusive of defect sites which are quite rare) (Ref. 22), and we might hope to get a very accurate measurement of λ.

However, there are two poorly understood effects which make interpretation of the experiments difficult. The first is the influence of interactions between paramagnetic ions on the alignment of Co^{58}. The second is the reorientation of the nucleus during the time between the β-decay (more precisely the K-electron capture) and the γ-ray emission. Experiments have determined the effect of ionic interactions;

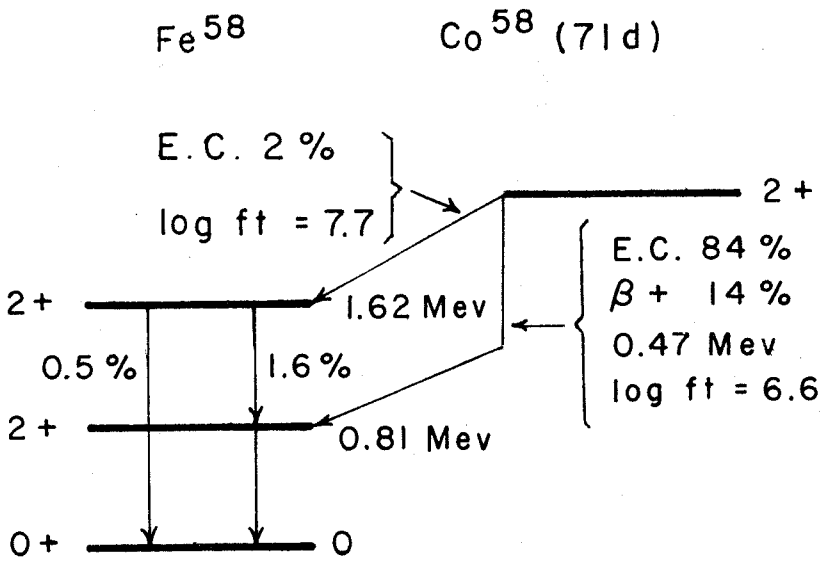

DECAY SCHEME OF Co^{58}

E. C. is electron capture.

From H. Fraunfelder et al (Ref. 18)

FIGURE 1

however no experiments have solved the problem of nuclear reorientation. Experiments are suggested which may shed some light on this subject.

I. APPARATUS

I.1 CRYOGENIC APPARATUS

a) Description

The radioactive $NiSiF_6 \cdot 6H_2O$ source crystal is grown by the method described in Appendix I. The crystal is glued and tied with thread onto the pedestal (Fig. 2). The correct design and assembly of this pedestal is essential to the optimum cryogenic performance of the entire system. After the demagnetization this glass support should insulate the crystal from the $1^{\circ}K$ helium bath. At the same time it must be strong enough so that in moving the Dewar system from the magnet to the counting position the crystal does not bang against the side of the sample chamber.

Some potassium chrome alum $Cr_2(SO_4)_3K_2SO_4 \cdot 24H_2O$ guard crystals are tied and glued onto the pedestal in several places. After demagnetization these crystals which are at $0.005^{\circ}K$ should pull the temperature of the pedestal at the point of attachment down to the order of $0.1^{\circ}K$. Glass this cold is a very good insulator, thus the heat flux into the source crystal is greatly decreased. How cold the pedestal becomes, however, depends on the manner in which these crystals are attached. Glue probably increases the thermal contact. However, the crystals are shaped and pulled tight with string in such a way as to provide the greatest possible area of direct contact. In some cases guard crystals are

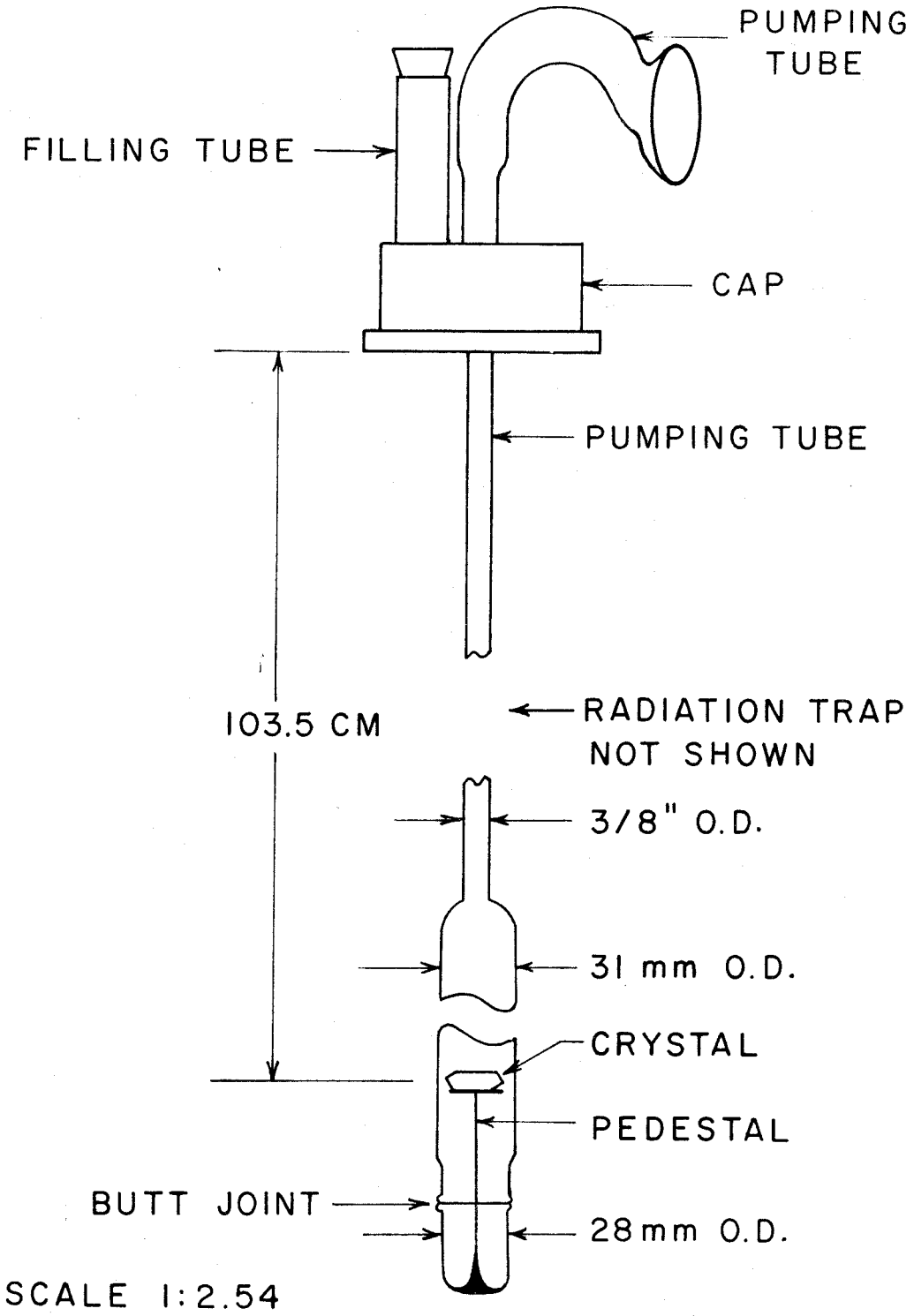

DEWAR CAP AND SAMPLE CHAMBER ASSEMBLY

FIGURE 2

placed on top of the source crystal. These serve to absorb possible thermal radiation from above. They also act as a getter for any helium gas which may be in the sample chamber before demagnetization.

The bottom section of the sample chamber is glued to the top section of the sample chamber with Epibond 101 epoxy resin. This joint has proven leak proof about 95% of the time when the ground glass surfaces of the butt joint were in anything but the worst condition. However, it is found that the temperature changes cause the Epibond to tear chips out of the Pyrex and after about ten to twenty gluings the ground glass may develop a pit extending from the outside to the inside. At this state the seal will fail occasionally.

Even a good seal is prone to fail if it is maintained at room temperature for as long as four days. This is because the epoxy hardens and is unable to take the thermal shock of cooling.

The Epibond joint is made by applying a thin, continuous ring of the epoxy to the carefully cleaned lower ground glass surface. Care is taken to avoid trapping air bubbles. This is then butted against the clean upper ground glass surface and a <u>partial</u> vacuum ($P > 5$ cm Hg) is pumped on the chamber. The hose to the pump is then closed off. After about 2 hours a bead of Epibond is run around the outside of the joint to seal possible leaks.

In the assembly care is taken so that particular crystal faces lie normal to the axis of the sample chamber. Other crystal faces are aligned in a known direction with respect to the sample chamber assembly for use later on in setting up the counters.

After the epoxy has cured at room temperature for about 12 hours the sample chamber is painted black with colloidal graphite. All of the glass work is checked to make sure that it is light tight. After attaching glass wool about one foot from the top of the pump-out tube* the assembly is placed in the Dewars and a black wax seal is made between the pump-out tube and the manifold on the boom. The boom swings between the counters and the magnet.

The Bitter type A. D. Little Co. iron magnet supplies a field of 21.8 kilogauss with 5-1/2" pole faces 2-5/16" apart. The current requirement for this field is 220 amps (at about 120 volts). At this point the magnet is almost saturated. Increasing the current by a factor of $\sqrt{2}$ would increase the field by 1000 gauss. The uniformity of the field is very good. It changes by 1.5% at 3 cm from the center, 5% at 5 cm, and 10.3% at 6 cm.**

---

*The glass wool is to damp out the strange sonic vibrations which transfer energy from the warm cap to the helium liquid.

**The maintenance of the magnet is simple but cannot be neglected. The cooling fluid level is kept halfway up the site glass. Tetraphenyltin is added with new fluid to prevent

The helium Dewar is connected by means of a large diameter pumping line to a Consolidated Vacuum KB 150-04 Booster Pump. This oil diffusion pump operates at 294°C. The line from this diffusion pump goes to a Kinney mechanical pump.

In addition to its being connected to the sample chamber, the manifold is also connected via stopcocks to an oil diffusion pump located on the boom, the helium Dewar, the vacuum space of the helium Dewar, pressure gauges, and an unconnected tygon tube. These multiple connections permit accurate gas handling both during the setting up of the experiment and during the experiment itself.

b) Operation of the cryogenic equipment

The system is cooled gradually over a period of 6 to 8 hours to liquid nitrogen temperature (77°K) in order to minimize thermal shock. When it is certain that the system is at nitrogen temperature a vacuum is pumped on the sample chamber. (Prolonged pumping on a warm sample chamber will dehydrate the crystal.) Only then is the main helium Dewar pumped on--this avoids the danger of a pressure differential

---

decomposition of the trichlorobenzene cooling fluid. The silica gel desiccant in the expansion tank should be changed occasionally. If the leakage resistance to ground across all the coils in the magnet is not better than 100K measured with an ohm meter, it may indicate deterioration of the coolant.

pulling the bottom off the sample chamber. After filling the main Dewar with helium gas and evacuating the transfer space between the helium and the nitrogen Dewars, liquid helium is transferred into the main helium Dewar. After the helium is pumped down to as low a temperature as it will reach ($0.95^{\circ}K$) and 5 to 50 microns of helium gas have been put in the sample chamber, the Dewars are put in the magnet and the magnet turned on.

The heat given off by the sample and guard crystals in this isothermal magnetization is transferred through the helium gas to the helium bath; about twelve minutes is allowed for this. The helium gas is then pumped out of the sample chamber removing the thermal linkage. The chamber is pumped down to about 10^{-5} mm with a pump-out time of 5 to 40 minutes.

Now the crystals can be adiabatically demagnetized--the magnetic field has already split the almost degenerate, paramagnetic energy levels by 1 or 2 k and the ratio of the population of the higher energy level to the population of the lower energy level is e^{-1} or e^{-2} (Maxwell-Boltzman Law). Clearly some of the randomness of the system has been removed. Since the entropy of a system is solely a measure of its randomness, the entropy has also decreased.

As the magnetic field is removed the splitting of the energy levels of the paramagnetic ions becomes smaller and

smaller. However, the ratio of the populations must remain the same as long as the ions can be considered as being independent because the randomness (entropy) would change if the independent ionic level populations were to change. Since the demagnetization is being done slowly (~2 sec) on a thermally isolated salt the entropy cannot change.

As the splitting which is proportional to the magnetic field decreases, the temperature must also decrease to maintain the same population distribution.

It may at first seem that the sample will cool to absolute zero when the field has been removed. Of course nature finds a way to prevent this. The unavoidable mechanism of inter-ionic coupling becomes important at low fields and the ions can no longer be treated as independent. The couplings split the approaching degeneracy and the salt stops cooling. The final temperature in zero field is the order of the ionic interactions. Appendix II gives quantitative data on the thermodynamics of demagnetization.

If the nuclear spin of the coolant ion is not zero some of the orderliness of the electron spin system will have to be sacrificed to order the nuclei. Thus the hyperfine interaction also limits the temperature achieved in zero fields.

When the field has been removed, the boom is carefully moved into the counting position where the desired number of cold γ-ray counts are taken. Then about 20 microns of helium

gas is introduced into the sample chamber. This establishes thermal contact with the bath and brings the sample quickly to 1°K. In these experiments alignment at 1°K is negligible, and warm counting rates are then taken. The Dewar is moved back into the magnet, and the next run is started.

I.2 COUNTERS AND ELECTRONICS

a) Description

When the Dewar is in counting position the sample is surrounded by four NaI(Tl) scintillation counters. These are arranged either all in a horizontal plane or with the two 45° counters in the plane determined by the vertical and the axis of alignment of the source. In either case, the biggest crystal (2" x 1-3/4" D) is in the 0° position measured with respect to the axis of nuclear alignment. The second largest (1" x 1-1/2" D) is in the 90° position, and the small ones (1" x 1" D) are at 45°.

A γ-ray absorbed in the NaI(Tl) causes a pulse of light proportional to the energy absorbed to be given off and to enter the photomultiplier tube. This causes a current pulse to arrive at the output of the light sensitive tube. This pulse, after cathode follower preamplification, is sent through twenty foot RG 114 cables to the counting room upstairs. Here the signal appears on the matched input of a linear amplifier.

In the case of the 0° and 90° counters the pulse is taken from the output of the linear amplifier and fed into a pulse height analyzer (Detectolab DZ15). For each pulse into the analyzer which falls within a given preset voltage interval a pulse appears on the output and triggers a scaler.

In the case of the 45° counters the pulses are taken from the pulse height selector output of the linear amplifier and fed directly to the scaler. Any linear amplifier input pulse above a certain preset level will trigger the scaler. The scaler is left on for the desired length of time, and the accumulated counts are recorded.

b) Stability of the electronics

In the coldest 15 minutes of the average run the order of 300,000 counts will be received using a 15 μcurie source. The counting statistics on this many counts will be $\pm\sqrt{\frac{1}{300,000}} = \pm 0.2\%$. Thus, it is clear that the electronics must be very stable in order to have these statistical errors meaningful. Once the pulse height analyzers are set so that the counter is looking at the 810 kev line, the gain of the system must not change by more than 1%. (This prohibits 1 volt fluctuations in the high voltage supply.) The channel width in the pulse height analyzer must be stable to 0.5%, and the base line to 1%.

These requirements are met, and fluctuations of 0.5% in counting rate are seldom observed. This is evidenced by the

consistency from run to run in the measured λ (Appendix VIII).

In order to obtain this stability it was found necessary to keep the electronics at a very constant temperature during a run. Hence, they were allowed to warm up for at least 24 hours, and there was no opening of doors and windows while experiments were under way. The ac line voltage was found to vary by as much as 8 volts during the day. For this reason runs were made only at night, and ac line regulators were used on all the sensitive equipment.

II THEORY FOR THE IDEAL CASE

II.1 THE NUCLEAR PROBLEM

If radioactive nuclei are oriented randomly in space then, of course, all radiation from these nuclei will be isotropic in space. However, if the nuclei are not oriented at random, then, in general, the expression for the angular distribution of radiations must be written as follows:

$$W(\theta,\phi) = 1 - \sum_{n=1} \sum_{m=0}^{n} C_n^m P_n^m(\cos\theta) \cos m(\phi - \delta_{m,n}) \quad (1)$$

θ is the polar angle measured with respect to a direction in space

ϕ is the azimuthal angle about this direction

$P_n^m(\cos\theta)$ are the Legendre polynomials

C_n^m are constants dependent on the choice of coordinates, alignment mechanism, temperature, and the mode of nuclear decay.

This expression is normalized to unit intensity in all directions for the unaligned nuclei. Note that since

$$\int_{\text{sphere}} P_n^m(\cos\theta)\, d\Omega = 0 \qquad \text{for} \qquad n > o \quad (2)$$

$$\int_{\text{sphere}} W(\theta,\phi)\, d\Omega = 4\pi \quad (3)$$

$d\Omega$ is an increment of solid angle

If there is axial symmetry about the polar axis, clearly equation 1 becomes:

$$W(\theta,\phi) = W(\theta) = 1 - \sum_{n=1} C_n P_n(\cos\theta) \qquad (4)$$

In almost all cases of interest, axial symmetry can be assumed. Therefore, unless otherwise noted, expression 4 will be used.

How do the C_n's depend on the mode of decay and the alignment parameters in the particular case of a γ-ray emitted after a β-decay (Fig. 3a)? Cox, Tolhoek, etc., (Ref. 23,24, 25,26) are the basic references for nuclear aspects of this problem. While they treat the axially symmetric nuclear problem in great generality, they only calculate the alignment parameters in the very simplest case. Their conclusions will be given here. In the next subsections the calculation of the alignment parameters will be considered in some detail.

First, let us assume that we know the alignment properties of level (i) immediately preceding the γ-decay of interest. In particular, examine the case where the magnetic quantum number (I_z) is a good quantum number. In addition let us assume that we know the relative populations ($a_{I_z^i}$) of the $2I^i + 1$ levels. (Note that the z-axis is the axis symmetry, and hence the axis of $\theta = 0$.) We thus have $2I^i$ independent numbers $a_{I_z^i}$ if we add the condition that (Ref. 23):

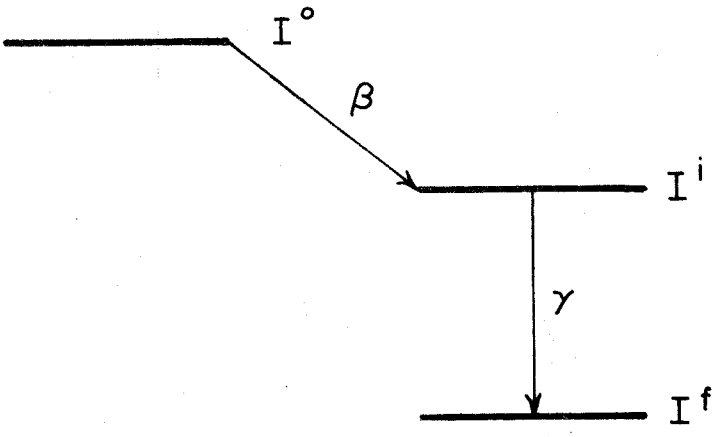

(a)

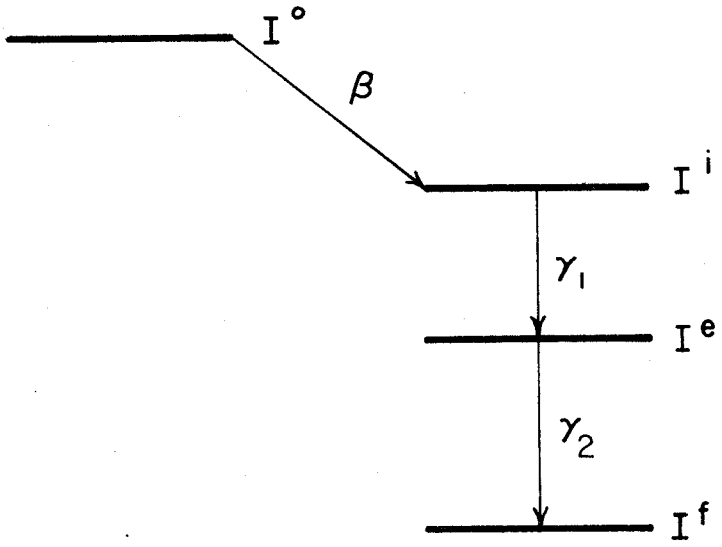

(b)

TYPICAL β-γ DECAY SCHEMES

FIGURE 3

$$\sum_{I_z^i} a_{I_z^i} = 1 \tag{5}$$

As a result of the calculations of Tolhoek and Cox (Ref. 23) the $a_{I_z^i}$ will always appear in combinations of the form $\sum_{I_z^i}(I_z^i)^k a_{I_z^i}$ (often called moments). We therefore define independent combinations of this form which are equivalent to the set of $2I^i$ independent numbers $a_{I_z^i}$

$$f_k^i = \sum_{\nu=0}^{k} \alpha_{k,\nu} \left[\sum_{I_z^i}(I_z^i)^\nu a_{I_z^i}\right] \qquad k \geq 1 \tag{6}$$

The $\alpha_{k,\nu}$ are chosen so that if the $a_{I_z^i}$'s are all equal $f_k^i = 0$. In addition reference 23 shows that

$$f_k^i = 0 \quad \text{if} \qquad k \geq 2I^i + 1 \tag{7}$$

We now, for convenience, shall describe the alignment in terms of the f_k^i's instead of the $a_{I_z^i}$'s. As a matter of fact, f_2^i and f_4^i are written as follows (Ref. 23):

$$f_2^i = (I^i)^{-2}\left[\sum_{I_z^i}(I_z^i)^2 a_{I_z^i} - \frac{1}{3} I^i(I^i+1)\right] \tag{8a}$$

$$f_4^i = (I^i)^{-4}\left\{\sum_{I_z^i}(I_z^i)^4 a_{I_z^i} - \frac{1}{7}\left[6(I^i)^2+6I^i-5\right]\sum_{I_z^i}(I_z^i)^2 a_{I_z^i} + \frac{3}{35}(I^i)(I^i-1)(I^i+1)(I^i+2)\right\} \tag{8b}$$

We now write down the equation for $W(\theta)$ in the case of dipole radiation (the γ-ray carries away 1 unit of angular momentum) and quadrupole (the γ-ray carries away 2 units) (Ref. 23):

Dipole:

$$\text{for } I_f = I_i - 1 \quad W(\theta) = 1 + \tfrac{3}{2} N_2^i f_2^i P_2(\cos\theta) \qquad (9a)$$

$$I_f = I_i \quad W(\theta) = 1 - \tfrac{3}{2} K_2^i f_2^i P_2(\cos\theta) \qquad (9b)$$

$$I_f = I_i + 1 \quad W(\theta) = 1 + \tfrac{3}{2} M_2^i f_2^i P_2(\cos\theta) \qquad (9c)$$

Quadrupole:*

$$\text{for } I_f = I_i - 2 \quad W(\theta) = 1 - \tfrac{15}{7} N_2^i f_2^i P_2(\cos\theta) - 5 N_4^i f_4^i P_4(\cos\theta) \qquad (10a)$$

$$I_f = I_i + 2 \quad W(\theta) = 1 - \tfrac{15}{7} M_2^i f_2^i P_2(\cos\theta) - 5 M_4^i f_4^i P_4(\cos\theta) \qquad (10b)$$

---

*We have not covered all possible cases of quadrupole emission. However, if $|I_f - I_i| \leq 1$ the γ-ray will either be dipole or a mixture of quadrupole and dipole radiation. The mixed transitions are covered by Tolhoek (Ref. 26).

where

$$P_2(\cos\theta) = \frac{3}{2}\left(\cos^2\theta - \frac{1}{3}\right) \tag{11a}$$

$$P_4(\cos\theta) = \frac{35}{8}\left(\cos^4\theta - \frac{6}{7}\cos^2\theta + \frac{3}{35}\right) \tag{11b}$$

$$N_k^i = b_k (I^i)^k (2I^i - k)!/(2I^i)! \tag{12a}$$

$$M_k^i = b_k (I^i)^k (2I^i + 1)!/(2I^i + k + 1)! \tag{12b}$$

$$K_2^i = I_i/I_i + 1 \tag{12c}$$

and where

$$b_k = 2^{\frac{1}{2}k} \quad \text{if } k \text{ is even} \tag{12d}$$

However, we still do not have the problem solved, because we must relate the alignment parameters for the intermediate state (i) to those of the initial state (o). Suppose that the radiation occurring between states o and i carries off L units of angular momentum. Then (Ref. 24):

$$\text{for } I_i = I_o - L \qquad N_k^i f_k^i = N_k^o f_k^o \tag{13a}$$

$$I_i = I_o + L \qquad M_k^i f_k^i = M_k^o f_k^o \tag{13b}$$

$$I_i = I_o \qquad f_k^i = \left[1 - \frac{k(k+1)}{2I^o(I^o+1)}\right] f_k^o \tag{13c}$$

$$L = 1$$

Thus, using equations 9, 10, 12, and 13 we can calculate $W(\theta)$ in terms of f_2^o and f_4^o in a wide number of cases--even for γ_2 in figure 3b. Of course, sometimes the cascades will not satisfy the conditions on equations 9, 10, and 12; however the more general tabulations referred to in (Ref. 24,25) will handle these cases.

In the case of the principal 810 kev line in Co^{58} $W(\theta)$ is (Appendix III):

$$W(\theta) = 1 - \frac{5}{7}(1+\lambda)f_2^o P_2(\cos\theta) + \frac{80}{9}(1 - \frac{5}{2}\lambda)f_4^o P_4(\cos\theta) \quad (14)$$

where λ is the fraction of the β-decays or K-captures which go by Fermi decay.

II.2 THE SPIN HAMILTONIAN

We can now predict $W(\theta)$ for a given λ if we can determine the alignment parameters f_2^o and f_4^o. We must examine the forces which act on the nucleus. Consider the various terms in the Hamiltonian describing an isolated paramagnetic ion in a crystal (Ref. 27). In order of decreasing magnitude (for the iron group elements) they are:

1. The coulomb interaction of the electrons with the fixed nucleus and with each other.
2. The term describing the effect of the crystal

electric field on the individual electrons.*

3. Interactions between the different electron spins and the different electron orbits (10^2 - 10^3k).
4. The term describing the effect of the external magnetic field interacting with the electrons.
5. The magnetic hyperfine term which couples the nuclear magnetic moment to the electronic magnetic field (10^{-2}k).
6. The nuclear electric quadruple term which couples the nuclear quadrupole moment to the gradient of the atomic electric field. This is the order of 10^{-4}k except for the uranium and transuranium elements where it may be ~ 1 k.
7. The coupling of the nucleus directly to the external magnetic field.

This complicated Hamiltonian is solved by obtaining from theory and experiment a representation which is diagonal in terms 1 of the Hamiltonian. Terms 2 are applied as a perturbation to obtain a new representation with a new energy level scheme. Then, terms 3 are applied on this new representation, etc. Finally, we are left with a long series of energy levels covering an enormous energy spectrum. We are not interested

---

*In the rare earth series the spin orbit term is larger than the crystal field term because the unpaired electrons which cause paramagnetism are not on the outside of the ion. Instead they are in inner orbits where they are shielded by outer electrons.

in levels which are more than ~1k above the ground level. The low levels can be described by an "effective spin Hamiltonian" ($\mathcal{H}$). The derivation of this $\mathcal{H}$ is long and involved and is covered by reference 27. A check on the validity of the spin Hamiltonian, as well as values for the numerical coefficients in $\mathcal{H}$, is obtained from paramagnetic resonance data. The most general spin Hamiltonian is as follows:

$$\begin{aligned}\mathcal{H} = {} & \beta\left(g_z H_z S_z + g_x H_x S_x + g_y H_y S_y\right) \\ & + D\left[S_z^2 - \tfrac{1}{3}(S)(S+1)\right] + E\left(S_x^2 - S_y^2\right) \\ & + A_z S_z I_z + A_x S_x I_x + A_y S_y I_y \\ & - g_n \beta_n \vec{H}\cdot\vec{I} + P\left[I_z^2 - \tfrac{1}{3}(I)(I+1)\right] + P'\left(I_x^2 - I_y^2\right)\end{aligned} \tag{15}$$

where

β is the Bohr magneton and β_n is the nuclear Bohr magneton

S_x, S_y, and S_z are electronic spin operators

I_x, I_y, and I_z are nuclear spin operators

S is the effective spin of these low lying levels

I is the total nuclear spin

H_x, H_y, and H_z are the magnetic fields in the indicated directions

And the other quantities are numerical coefficients.

The first term describes the interaction of the electron spin with the magnetic field. The "D" and "E" terms are due to the effect of the crystalline field on the electron orbits and in turn on the spins. If $S = \frac{1}{2}$ these terms do not contribute.

The "A" terms describe the magnetic coupling between the nuclear moment and the magnetic field of the electron at the nucleus. The "P" terms couple the nuclear quadrupole moment to the gradient of the ionic electric field at the nucleus. The "g_n" term connects the nuclear spin to the external magnetic field.

For traces of Co^{59} $SiF_6 \cdot 6H_2O$ in pure diamagnetic $ZnSiF_6 \cdot 6H_2O$ at 20°K resonance data (Ref. 21) shows that the Hamiltonian is:

$$\mathcal{H} = g_{\parallel} \beta H_z S_z + g_{\perp} \beta (H_x S_x + H_y S_y) + A S_z I_z + B(S_x I_x + S_y I_y) \tag{16}$$

where

$$g_{\parallel} = 5.82 \pm 0.12$$
$$g_{\perp} = 3.44 \pm 0.07$$
$$A = 0.0184 \pm 0.0004 \text{ cm}^{-1}$$
$$B = 0.0047 \pm 0.0002 \text{ cm}^{-1}$$

and

$$S = \text{effective electronic spin} = \frac{1}{2}$$

I = total nuclear spin of Co^{59} is $\frac{7}{2}$

Several comments about this expression are necessary.

1. The notation has been changed from equation 15 to be more appropriate to the axial symmetry involved.
2. $S = \frac{1}{2}$ means "D" and "E" terms in equation 15 are zero because $S_z^2\varphi = S_x^2\varphi = S_y^2\varphi = \frac{1}{4}\varphi = \frac{1}{3}S(S+1)\varphi$ if φ is any wave function of a spin $\frac{1}{2}$ particle. (Operate on any wave function with equation 18a or 18b squared.)
3. "P" and "$\vec{H}\cdot\vec{I}$" are too small to be observed.
4. This expression is in terms of cm^{-1} instead of degrees Kelvin times k and the expression is for Co^{59} instead of Co^{58}.

After correcting units, and adjusting the parameters to Co^{58} (Appendix IV) we obtain the Hamiltonian for Co^{58} nuclei of independent ions in $ZnSiF_6 \cdot 6H_2O$:

$$\mathcal{H}/k = 3.91 \times 10^{-4} H_z S_z + 2.31 \times 10^{-4} (H_x S_x + H_y S_y) + 0.0403 S_z I_z + 0.0103 (S_x I_x + S_y I_y) \quad (17)$$

where H_z, H_x, and H_y are in gauss and $\mathcal{H}/k$ is in degrees Kelvin.

II.3 DIAGONALIZATION OF THE SPIN HAMILTONIAN

In order to use the spin Hamiltonian to derive the quantities f_2^o and f_4^o for Co^{58} it must first be diagonalized.*

*In some approximate methods this may be avoided. (Appendix IX).

This will give the energy levels and the eigenstates of the Hamiltonian. Using Maxwell-Boltzman statistics we can obtain the populations a_{I_z}. (For convenience we have left off the o denoting the initial state.)

We choose as our representation states which are diagonal in S_z and I_z. They are $|S_z, I_z\rangle$ using the Dirac notation ($S_z = +\frac{1}{2}, -\frac{1}{2}$; $I_z = 2,1,0,-1,-2$). We recall several properties of the spin operators (Ref. 21).

$$S_x = \frac{S_+ + S_-}{2} \tag{18a}$$

$$S_y = \frac{S_+ - S_-}{2i} \tag{18b}$$

and that

$$S_+ |M\rangle = [S(S+1) - M(M+1)]^{\frac{1}{2}} |M+1\rangle \tag{19a}$$

$$S_- |M\rangle = [S(S+1) - M(M-1)]^{\frac{1}{2}} |M-1\rangle$$

The same properties hold for I_x and I_y.

Because the external field in these experiments is zero and because we are not considering ionic interactions we write $\mathcal{H}$ (Eq. 17) as:

$$\mathcal{H} = AS_zI_z + B(S_xI_x + S_yI_y) \tag{20}$$

where

$$A/k = 0.0403 \text{ degrees}$$

$$B/k = 0.0103 \text{ degrees}$$

Using equations 18a and 18b, equation 20 becomes

$$\mathcal{H} = AS_z I_z + B/2(S_+ I_- + S_- I_+) \tag{21}$$

An eigenstate, (ψ_μ) of this Hamiltonian can be written as follows:

$$\psi_\mu = \sum_{S_z, I_z} b_{\mu S_z I_z} |S_z, I_z\rangle \tag{22}$$

and because it is an eigenstate:

$$\mathcal{H}\,\psi_\mu = E_\mu \psi_\mu \tag{23}$$

In order to find the b's and the E's we write down the energy matrix of $\mathcal{H}$ as:*

---

*A typical element, for instance, column 1/2,1 , row -1/2,2 , is:

$$\langle 1/2,1|\mathcal{H}|-1/2,2\rangle = A\langle 1/2,1|\, S_z I_z|\, -1/2,2\rangle + \frac{B}{2}\langle 1/2,1\,|\, S_+ I_- + S_- I_+\,|\, -1/2,2\rangle$$

Using definition of S_z and equations 19a and 19b we have

$$\begin{aligned}\langle 1/2,1|\mathcal{H}|-1/2,2\rangle &= A\langle 1/2,1\,|\, -1/2 I_z\,|\, -1/2,2\rangle \\ &\quad + \frac{B}{2}\langle 1/2,1\,|\, 1I-\,|\, +1/2,2\rangle \\ &= A\langle 1/2,1\,|\, -1/2\cdot 2\,|\, -1/2,2\rangle \\ &\quad + \frac{B}{2}\langle 1/2,1|\, 1\cdot 2\,|+\,1/2,1\rangle \\ &= -A\langle 1/2,1\,|\, -1/2,2\rangle \\ &\quad + B\,\langle 1/2,1\,|\,1/2,1\rangle\end{aligned}$$

because of the orthonormality of the $|S_z, I_z\rangle$ representation we have

$$\langle 1/2,1\,|\,\mathcal{H}\,|\,-1/2,2\rangle = B$$

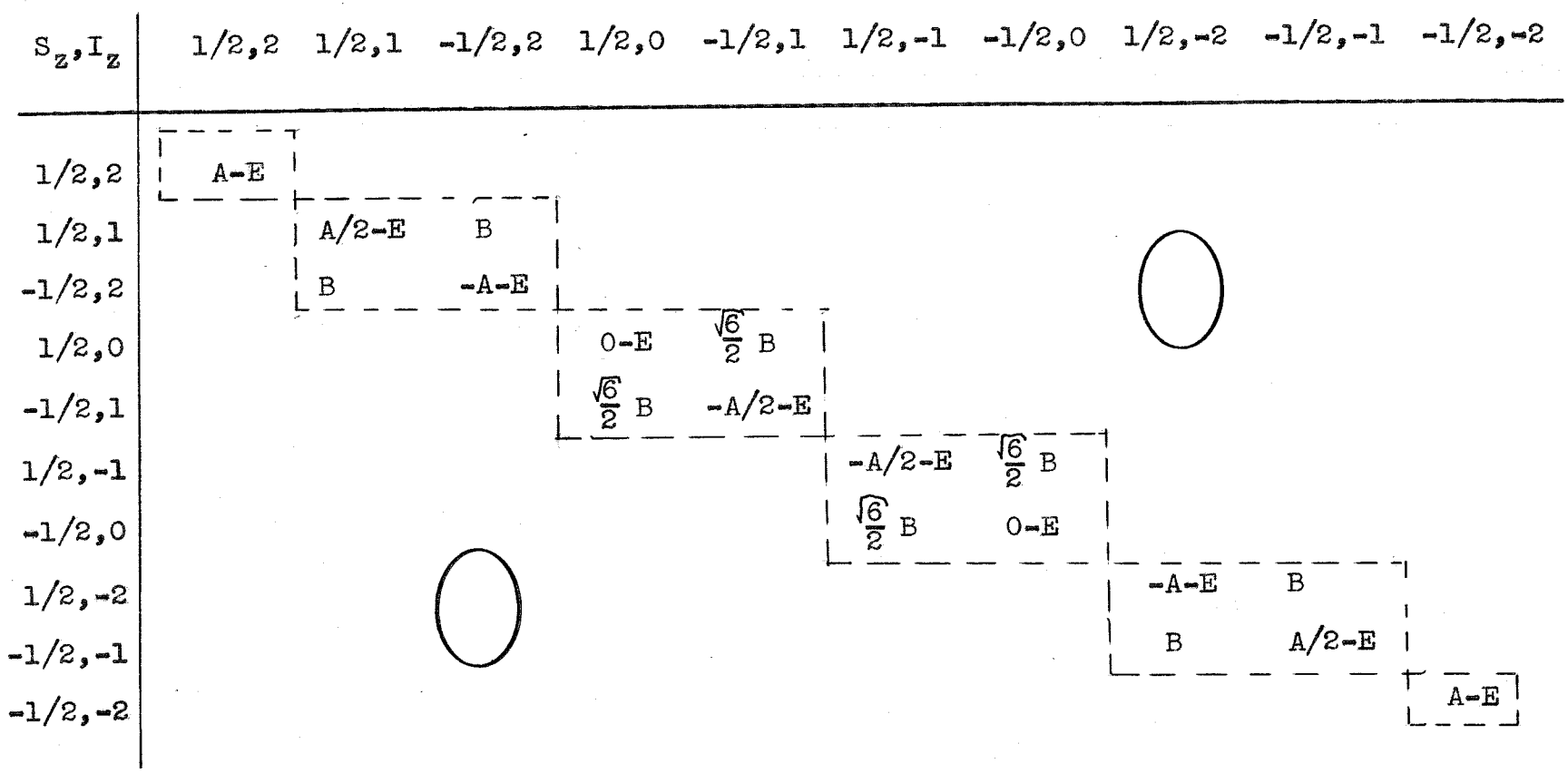
S_z, I_z
1/2,2 1/2,1 -1/2,2 1/2,0 -1/2,1 1/2,-1 -1/2,0 1/2,-2 -1/2,-1 -1/2,-2
1/2,2
1/2,1
-1/2,2
1/2,0
-1/2,1
1/2,-1
-1/2,0
1/2,-2
-1/2,-1
-1/2,-2
A-E
A/2-E B
B -A-E
0-E $\frac{\sqrt{6}}{2}$ B
$\frac{\sqrt{6}}{2}$ B -A/2-E
-A/2-E $\frac{\sqrt{6}}{2}$ B
$\frac{\sqrt{6}}{2}$ B 0-E
-A-E B
B A/2-E
A-E

The eigenvalues are the roots, E, obtained by setting the determinant of this matrix equal to zero. Since there are no elements mixing states between the boxes, we can simply set the determinant of each individual box equal to zero. A typical eigenstate is simply $\psi_i = \alpha|1/2, 1\rangle + \beta|-1/2, 2\rangle$

where $$(\alpha)(A/2 - F_\mu) + \beta(B) = 0 \qquad (24)$$

and

$$\alpha^2 + \beta^2 = 1 \qquad (25)$$

Table 1 gives a list of the ten eigenvalues and the ten eigenvectors obtained. Table 2 gives the same thing in the specific case of B/A equal to $\frac{1}{4}$ as given by equation 17. Figure 4 shows the corresponding energy level diagram.

II.4 STATISTICAL MECHANICS

Because the Co^{58} ions are assumed to be independent, we can draw an imaginary sphere around a typical ion and discuss the probability (P_μ) of its being in eigenstate (μ) of energy E_μ (Fig. 4).

Using Maxwell-Boltzman statistics we see that:

$$P_\mu = e^{-E_\mu/kT} \Big/ \sum_\eta e^{-E_\eta/kT} \qquad (26)$$

where

The summation on η is over all ten eigenvalues.

Table 1

Energies and Un-normalized Wave Functions for S = 1/2; I = 2. $\mathcal{H} = A(S_z I_z) + B(S_x I_y + S_y I_y)$.

E_1	$= A$		ψ_1	$= 1$	$\lvert 1/2,2\rangle$		
E_2	$= -A/4 + \sqrt{(3/4A)^2 + B^2}$		ψ_2	$= -B$	$\lvert 1/2,1\rangle$	$+ \left(3/4A - \sqrt{(3/4A)^2 + B^2} \right)$	$\lvert -1/2,2\rangle$
E_3	$= -A/4 + \sqrt{(1/4A)^2 + 3/2\ B^2}$		ψ_3	$= -B\sqrt{\frac{3}{2}}$	$\lvert 1/2,0\rangle$	$+ \left(1/4A - \sqrt{(1/4A)^2 + 3/2\ B^2} \right)$	$\lvert -1/2,1\rangle$
E_4	$= -A/4 + \sqrt{(1/4A)^2 + 3/2\ B^2}$		ψ_4	$= -B\sqrt{\frac{3}{2}}$	$\lvert 1/2,-1\rangle$	$+ \left(-1/4A - \sqrt{(1/4A)^2 + 3/2\ B^2} \right)$	$\lvert -1/2,0\rangle$
E_5	$= -A/4 + \sqrt{(3/4A)^2 + B^2}$		ψ_5	$= -B$	$\lvert 1/2,-2\rangle$	$+ \left(-3/4A - \sqrt{(3/4A)^2 + B^2} \right)$	$\lvert -1/2,-1\rangle$
E_6	$= A$		ψ_6	$=$		1	$\lvert -1/2,-2\rangle$
E_7	$= -A/4 - \sqrt{(3/4A)^2 + B^2}$		ψ_7	$= -B$	$\lvert 1/2,-2\rangle$	$+ \left(-3/4A + \sqrt{(3/4A)^2 + B^2} \right)$	$\lvert -1/2,-1\rangle$
E_8	$= -A/4 - \sqrt{(1/4A)^2 + 3/2\ B^2}$		ψ_8	$= -B\sqrt{\frac{3}{2}}$	$\lvert 1/2,-1\rangle$	$+ \left(-1/4A + \sqrt{(1/4A)^2 + 3/2\ B^2} \right)$	$\lvert -1/2,0\rangle$
E_9	$= -A/4 - \sqrt{(1/4A)^2 + 3/2\ B^2}$		ψ_9	$= -B\sqrt{\frac{3}{2}}$	$\lvert 1/2,0\rangle$	$+ \left(1/4A + \sqrt{(1/4A)^2 + 3/2\ B^2} \right)$	$\lvert -1/2,1\rangle$
E_{10}	$= -A/4 - \sqrt{(3/4A)^2 + B^2}$		ψ_{10}	$= -B$	$\lvert 1/2,1\rangle$	$+ \left(3/4A + \sqrt{(3/4A)^2 + B^2} \right)$	$\lvert -1/2,2\rangle$

Table 2

Energies and Normalized Wave Functions of Table 1 in the Case B/A = 1/4.

Energies	Normalized Wave Functions
$E_1 = 1.0000$ A	$\psi_1 = 1 \lvert 1/2,2\rangle$
$E_2 = 0.5406$ A	$\psi_2 = -\sqrt{0.973} \lvert 1/2,1\rangle - \sqrt{0.027} \lvert -1/2,2\rangle$
$E_3 = 0.1453$ A	$\psi_3 = -\sqrt{0.817} \lvert 1/2,0\rangle - \sqrt{0.183} \lvert -1/2,1\rangle$
$E_4 = 0.1453$ A	$\psi_4 = -\sqrt{0.183} \lvert 1/2,-1\rangle - \sqrt{0.817} \lvert -1/2,-0\rangle$
$E_5 = 0.5406$ A	$\psi_5 = -\sqrt{0.027} \lvert 1/2,-2\rangle - \sqrt{0.973} \lvert -1/2,-1\rangle$
$E_6 = 1.0000$ A	$\psi_6 = + 1 \lvert -1/2,-2\rangle$
$E_7 = -1.0406$ A	$\psi_7 = -\sqrt{0.973} \lvert 1/2,-2\rangle + \sqrt{0.027} \lvert -1/2,-1\rangle$
$E_8 = -0.6453$ A	$\psi_8 = -\sqrt{0.817} \lvert 1/2,-1\rangle + \sqrt{0.183} \lvert -1/2,0\rangle$
$E_9 = -0.6453$ A	$\psi_9 = -\sqrt{0.183} \lvert 1/2,0\rangle + \sqrt{0.817} \lvert -1/2,1\rangle$
$E_{10} = -1.0406$ A	$\psi_{10} = -\sqrt{0.027} \lvert 1/2,1\rangle + \sqrt{0.973} \lvert -1/2,2\rangle$

These apply to Co^{58} in $ZnSiF_6 \cdot 6H_2O$ in zero magnetic field.

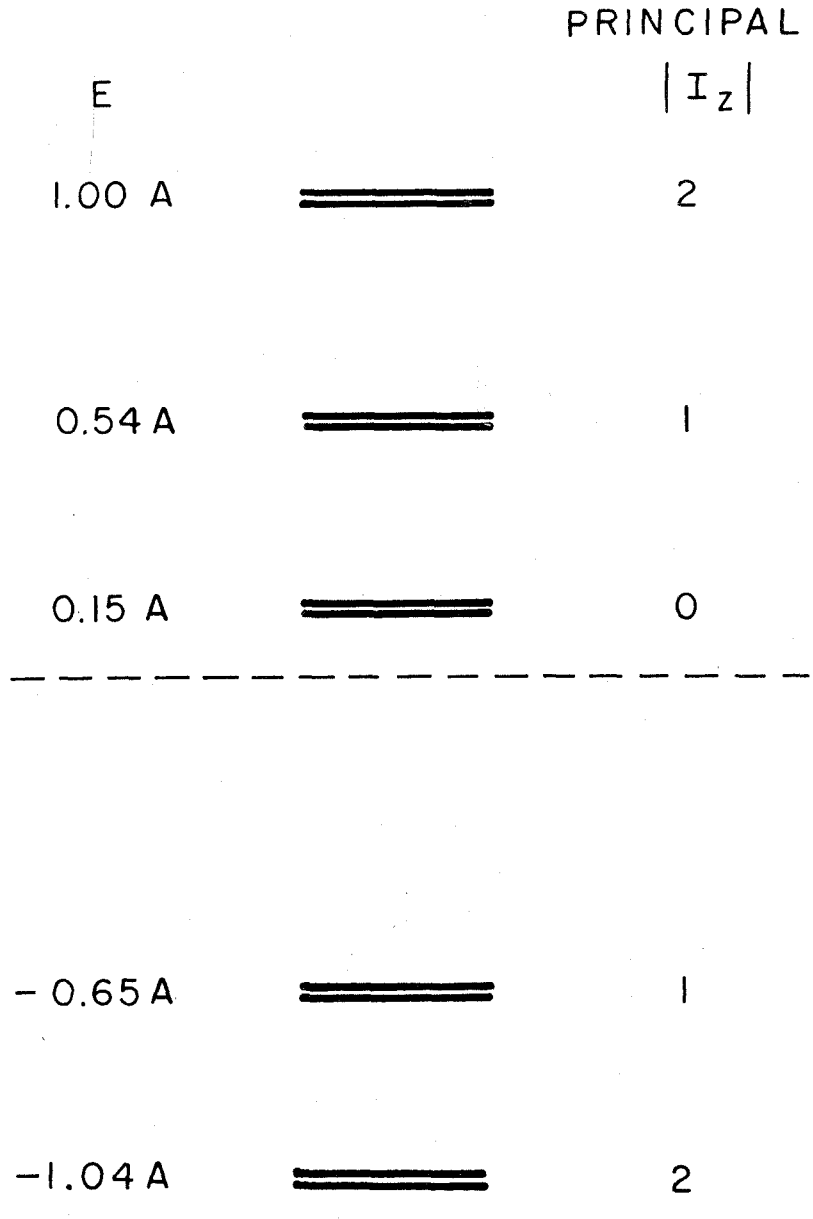

ENERGY LEVELS OF Co^{58} IN $ZnSiF_6 \cdot 6H_2O$

WITH NO MAGNETIC FIELD

From Table 2, preceding page. $A/k = 0.04^{\circ}K$.

FIGURE 4

Note that

$$\sum_{\mu} P_{\mu} = 1 \tag{27}$$

When the energy eigenstates are mixed the expression $\sum_{I_z} (I_z)^k a_{I_z}$ of equation 8 (p. 19) must be written more generally. We want the statistical average of the quantum operator $(I_z)^k$. Appendix V shows this to be $\sum_{\mu} a_{\mu} \langle (I_z)^k \rangle_{\mu}$.

Using this fact, along with equations 22 and 23 and allowing mixing of many states we have that:

$$\sum_{\mu} a_{\mu} \langle (I_z)^k \rangle_{\mu} = \frac{\sum_{S_z'} \sum_{I_z'} \sum_{\mu} (I_z')^k (e^{-E_{\mu}/kT}) (b_{\mu S_z' I_z'})^2}{\sum_{\eta} e^{-E_{\eta}/kT}} \tag{28}$$

Hence, using these sums in equations 8a and 8b in place of $\sum_{I_z} a_{I_z} (I_z)^k$ we can obtain $W(\theta)$ as a function only of and of temperature merely by substituting these values of f_2 and f_4 into equation 14.

Table 3 shows calculated values of $W(0^o)$, $W(45^o)$, and $W(90^o)$ for various λ's and various β's:

$$\beta = A/2kT \tag{29}$$

These results for 0^o and for 90^o are also plotted graphically (Fig. 5). The same graph contains several points for the

Table 3

Theoretical Values for $W(0^\circ)$, $W(45^\circ)$, and $W(90^\circ)$ for the Intense 810 kev Line of Co^{58} in $ZnSiF_6 \cdot 6H_2O$ (based on ideal theory)

	$\lambda = -0.1$			$\lambda = 0.0$			$\lambda = 0.1$		
	$W(0^\circ)$	$W(45^\circ)$	$W(90^\circ)$	$W(0^\circ)$	$W(45^\circ)$	$W(90^\circ)$	$W(0^\circ)$	$W(45^\circ)$	$W(90^\circ)$
.8	.9169	.9737	1.0488	.9050	.9719	1.0533	.8932	.9700	1.0577
1.00	.8969	.9626	1.0672	.8799	.9606	1.0725	.8629	.9587	1.0779
1.33	.8764	.9435	1.0958	.8506	.9423	1.1020	.8248	.9409	1.1080
1.50	.8717	.9344	1.1089	.8416	.9336	1.1150	.8114	.9327	1.1211
2.50	.8733	.8998	1.1681	.8220	.8927	1.1725	.7707	.8956	1.1775
3.00	.8790	.8750	1.1870	.8206	.8794	1.1907	.7622	.8837	1.1947
	.8972	.8394	1.2312	.8218	.8476	1.2330	.7464	.8557	1.2347

The following spin Hamiltonian is assumed: $\mathcal{H} = A(S_z I_z) + B(S_x I_x + S_y I_y)$

$B/A = 1/4$

$\beta = A/2kT$

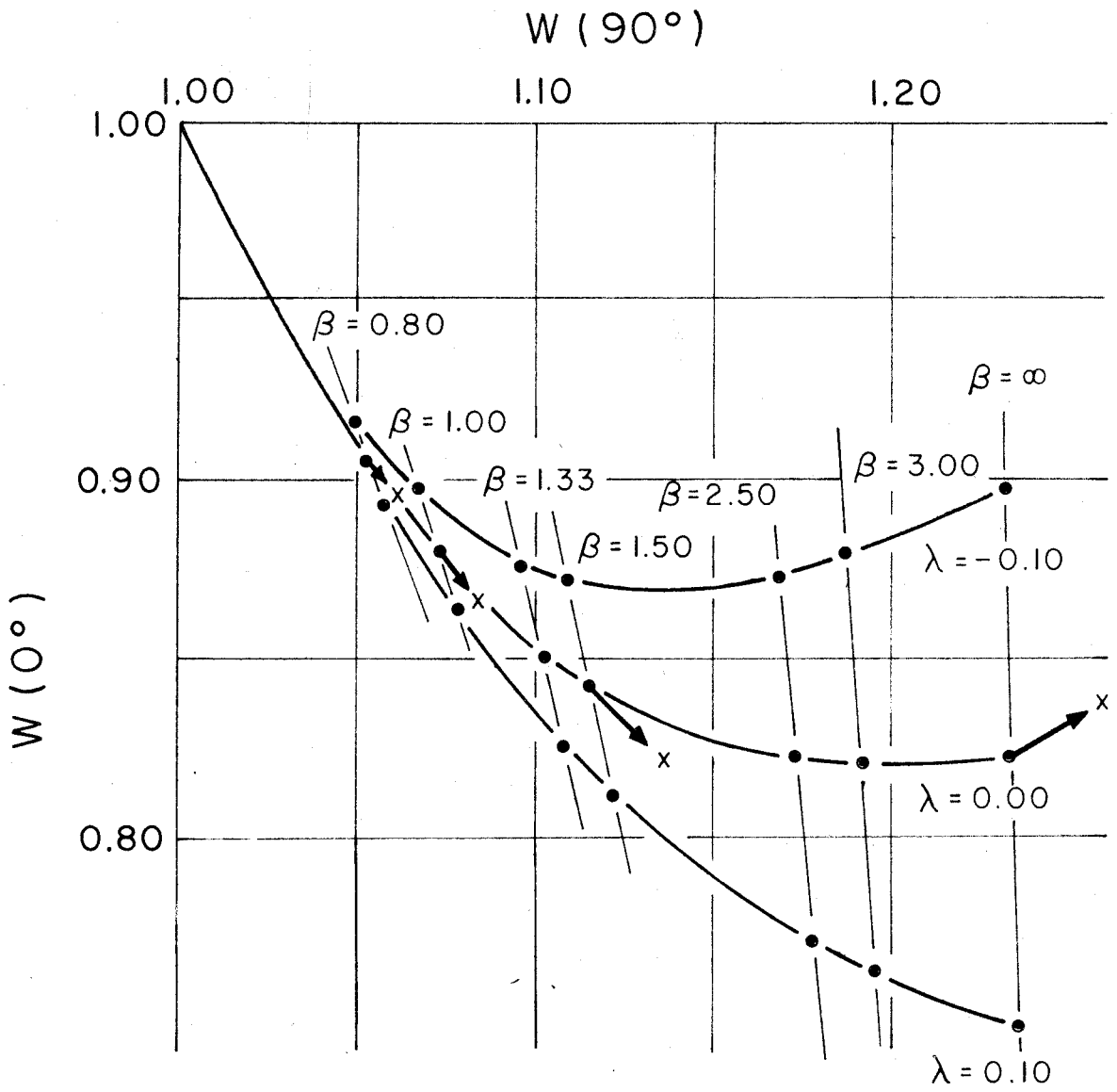

THEORETICAL NORMALIZED Co^{58} COUNTING RATES AT 0° W(0°) AND AT 90° W(90°) . $ZnSiF_6 \cdot 6H_2O$ WITH NO INTERACTIONS AND NO K-CAPTURE DEALIGNMENT

The spin Hamiltonian is:

$$\mathcal{H} = AS_zI_z + B(S_xI_x + S_yI_y)$$

$$B/A = 1/4$$

$$\beta = A/2kT$$

The arrows indicate the effect on certain theoretical points of letting B/A become zero, holding β and λ constant.

FIGURE 5

case B = 0, when there is no mixing of states and the energy levels are evenly spaced (Ref. 25). Note that this table and figure contain theoretical points calculated using a negative λ. While the definition of λ precludes negative values, additional factors combine to give "apparent" negative λ's experimentally.

Several interesting properties of this graph will be stated without proof:

1. For given values of f_2 and f_4 (and therefore β) the locus of points formed by varying λ is a straight line. The distance between $\lambda = \lambda_1$, and $\lambda = \lambda_2$ on this line is proportional to $(\lambda_1 - \lambda_2)$. The above is exactly true, and can be demonstrated from equation 14.
2. For a given λ and $\beta \left(= \frac{A}{2kT}\right)$ the locus of points formed by varying B/A lie in a straight line for small B/A. The distance between $(B/A) = (B/A)_1$ and $B/A = (B/A)_2$ is proportional to $(B/A)_2^2 - (B/A)_1^2$. This is shown by deriving f_2 and f_4 as a function of if B/A = 0, and then including the effect of B/A as a perturbation. Deviations from this approximation are insignificant at B/A = 1/4.
3. In the high temperature region, f_2 is proportional to T^{-2} and f_4 is proportional to T^{-4}, as can be shown by an expansion of f_2 and f_4 as a power series in (T^{-1}).

It is now possible to obtain an experimental value of λ by measuring $W(\theta)$ at any two angles, plotting the values obtained on a graph similar to figure 5 and determining what value of λ best fits the data.

III EXPERIMENTAL RESULTS

III.1 OBJECTIVE

We would like to obtain an accurate value for the nuclear λ. In an attempt to do this our first experiments aligned Co^{58} in crystals containing 6%, 12%, and 19% nickel. Comparing the experimental γ-ray angular distributions to the previous theory we obtained apparent values for λ. These experiments (discussed in Section III.3) yielded λ's which varied with nickel concentration, and which in most cases were negative. Since by definition λ expresses the fraction of Fermi type β-decay, the consistent appearance of negative values constituted a paradox requiring an examination on some other basis.

It was now apparent that ionic interactions were in some way disturbing the nuclear alignment. Thus, in order to obtain a true nuclear λ it was necessary to align the Co^{58} in a crystal which was free of paramagnetic material. Because the crystal had to be cooled to $\sim 0.02^{\circ}K$ this necessitated indirect cooling of the crystal, - until then only successful in cooling to about $0.1^{\circ}K$. However, using a different approach it was possible to cool a crystal containing a nominal 0% nickel to $\sim 0.012^{\circ}K$. These experiments are discussed in Section III.4.

III.2 EXPERIMENTAL METHOD

After a crystal of the desired type has been grown, mounted, and cooled from room temperature to $\sim 1^{\circ}K$, a series of demagnetizations ("runs") is made. For each run a series of simultaneous measurements of the γ-counting rates along the axis of symmetry, perpendicular to the axis of symmetry and at $\pm 45^{\circ}$ with respect to the axis of symmetry is obtained while the sample is cold following the demagnetization. When the sample has warmed up to where no accurate measurement of λ is possible, helium gas is introduced into the sample chamber to warm the sample to $0.95^{\circ}K$. Additional warm counts are then taken. The uncorrected normalized counting rates $W(0^{\circ})$, $W(90^{\circ})$, and $W(\pm 45^{\circ})$ are obtained by dividing a particular counting rate by the warm counting rate. Corrections are then made to take into account the weak competing Co^{58} γ-rays (Appendix VI). Appendix VII discusses the corrections for the finite solid angle of the counters, the measured counter noise, and the contamination of Co^{60} in the sample. The data is processed by plotting values of $W(0^{\circ})$ and $W(90^{\circ})$ on a graph containing the theoretical $W(0^{\circ})$ vs. $W(90^{\circ})$ curves of figure 5 (p. 36). These curves are plotted for different λ's. Points from many demagnetizations are plotted on the same graph. Each point is assigned a λ and a statistical error. It is also placed in one of five temperature ranges. All the points in a range are then statistically averaged to give a λ for each range. These

results are tabulated at the end of this section in Table 5. They are also given graphically in figures 6, 8, and 10. The assigned errors include statistics and possible shifts in the electronics (Appendix VIII). When in the first demagnetizations of a crystal the asymmetry in the two 45° counting rates indicated that the sample was misaligned by more than a few degrees in either the vertical or horizontal planes the counters were repositioned, and correct alignment observed. If there was any chance of the previous data being incorrect because of misalignment, it was discarded.

The 45° data was also checked to see if it was consistent with the 0° and 90° data. If $W(0^\circ)$ and $W(90^\circ)$ are known, and if it is assumed that only $P_2(\cos\theta)$ and $P_4(\cos\theta)$ terms are involved in the expression for $W(\theta)$, then $W(\theta)$ is determined. We set the observed $W(+45) + W(-45)/2$ equal to a $W(\theta')$ predicted from $W(0^\circ)$ and $W(90^\circ)$. The derived θ' is given in Table 4.

III.3 6%, 12%, AND 19% Ni CRYSTALS

These crystals were uniform in nickel concentration and in Co^{58} concentration throughout. The molar nickel concentration was obtained from chemical analysis. The crystals were grown from saturated water solutions with molar nickel-zinc ratios of 0.043, 0.085, and 0.17 respectively. The weights of the crystals were 2.8 gms, 3 gms, and 2.1 gms. Each contained about 15 μcuries of Co^{58}. See Appendix I.

Table 4

Derived Angle of 45° Counters Obtained from $\frac{W(+45^{\circ}) + W(-45^{\circ})}{2}$

Crystal	Derived Angle(θ') with Counters in Horizontal Plane (in degrees)	Derived Angle(θ') with Counters in Vertical Plane (in degrees)
6%	45.3 ± 0.3	46.2 ± 0.8
12%	44.0 ± 1.0	42.5 ± 2.0
19%	44.3 ± 0.2	---
0% (first)	44.3 ± 0.5	47.6 ± 0.6
0% (second)	48.5 ± 0.8	48.5 ± 0.5
4%	47.4 ± 2.0	45.0 ± 0.7

The results of these experiments, after all corrections, are shown in figure 6.* The measurements for these concentrations were obtained by 11, 4, and 4 demagnetizations respectively. As previously mentioned, the points shown represent the average of many points in the same "apparent" temperature range. The ranges are: $\beta < 1.00$; $1.00 < \beta < 1.3$; $1.3 < \beta < 1.6$; $1.6 < \beta < 2$; and $2 < \beta$.

III.4 TWO 0% Ni CRYSTALS

In an attempt to measure the real nuclear λ in an environment free of interaction effects, two differently constructed crystals were grown with the nickel and Co^{58} separated in space (Fig. 7). The first crystal weighs 2.3 gms and contains 4 μcuries; the second weighs 1.9 gms and contains 1.8 μcuries.

If the crystal conducts heat well enough, the section of the crystal containing the Co^{58} will be cooled by the nearby 12% material after demagnetization. This effect was actually observed and good alignments were obtained. The results of these experiments again grouped in temperature, and averaged are shown in figure 8.

The interpretation of the 0% nickel measurements must be made with caution. There is the problem that the Co^{58}

---

*Dagley et al. (Ref. 28) obtain $\lambda = -0.003 \pm 0.005$ using a crystal which they designate as (0.10 Ni, 0.90 Zn) $ZiF_6 \cdot 6H_2O$. However, it is most likely grown from a 15% Ni solution (Ref. 29) which would give us a 17% Ni crystal.

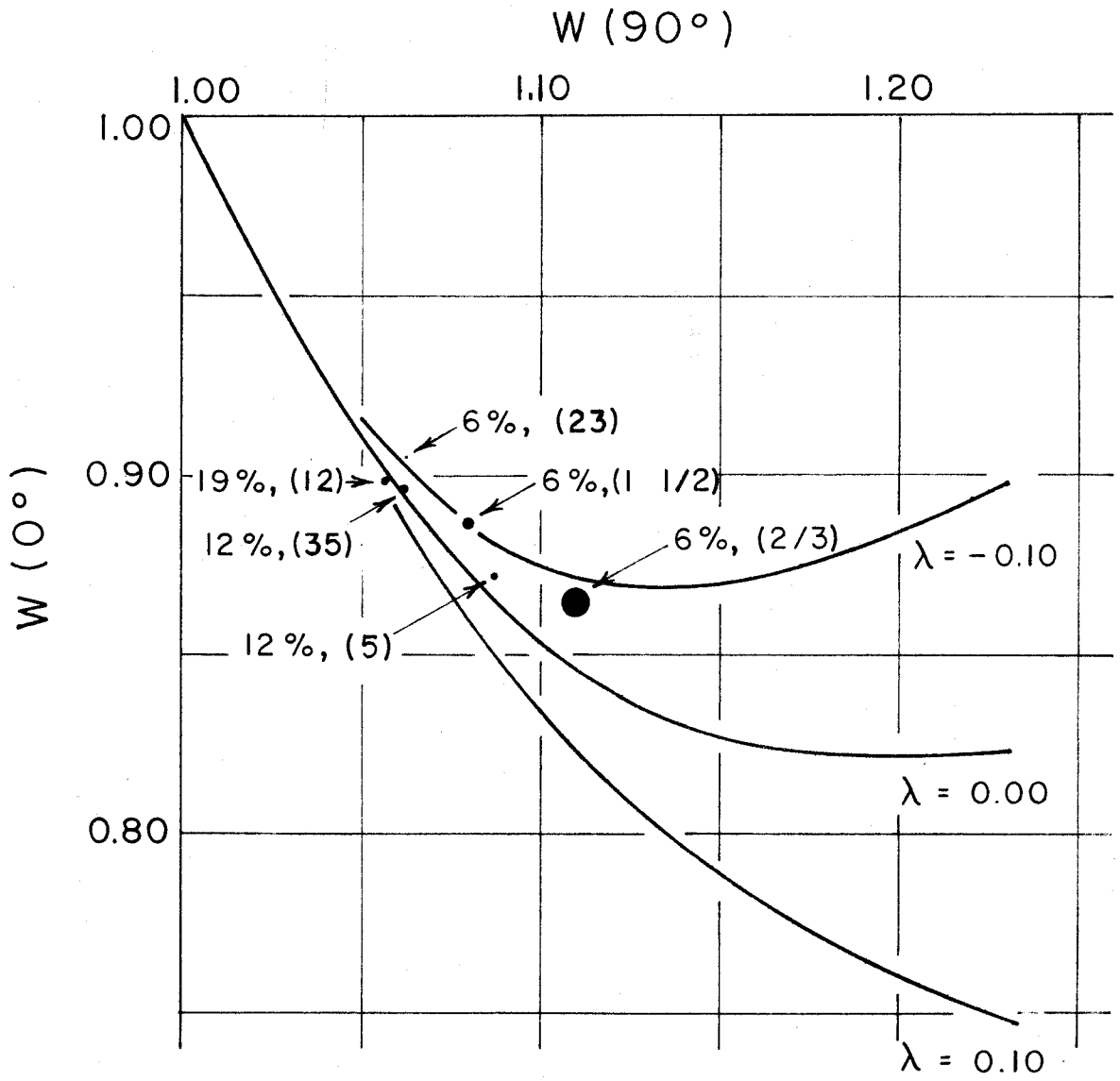

W(0°) VERSUS W(90°) FOR 6%, 12%, AND 19% Ni UNIFORM CRYSTALS

The number in parenthesis associated with each point represents the average time in minutes for the sample to warm up to that temperature.

The size of the point represents both statistical counting error and uncertainties associated with shifts in the electronics, etc. (See Appendix VIII).

Curves are for no interactions or K-capture dealignment.

The curves show the ideal theoretical relations of Section II.

FIGURE 6

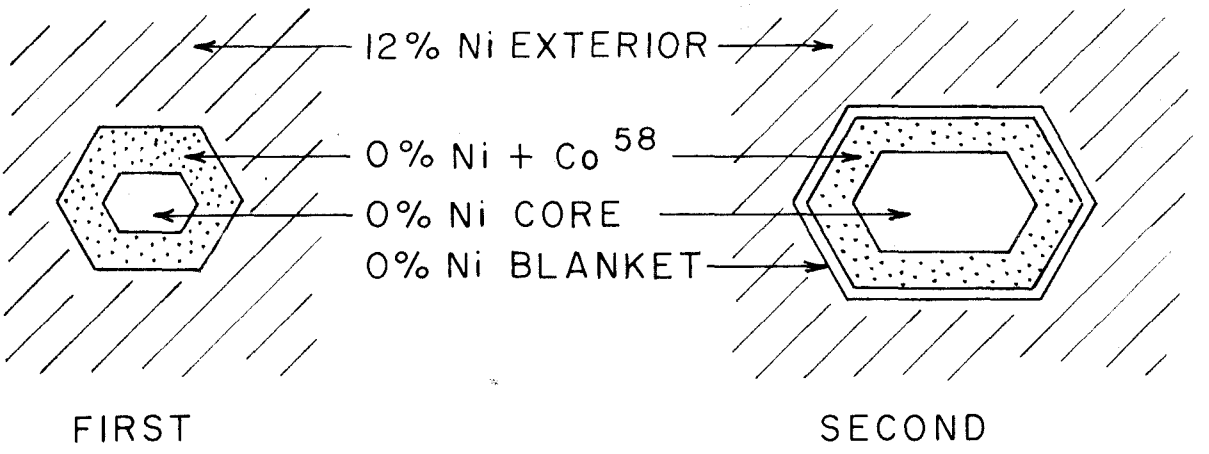

SCALE 10:1

STRUCTURE OF 0% Ni CRYSTALS

Cross section perpendicular to the axis of alignment

FIGURE 7

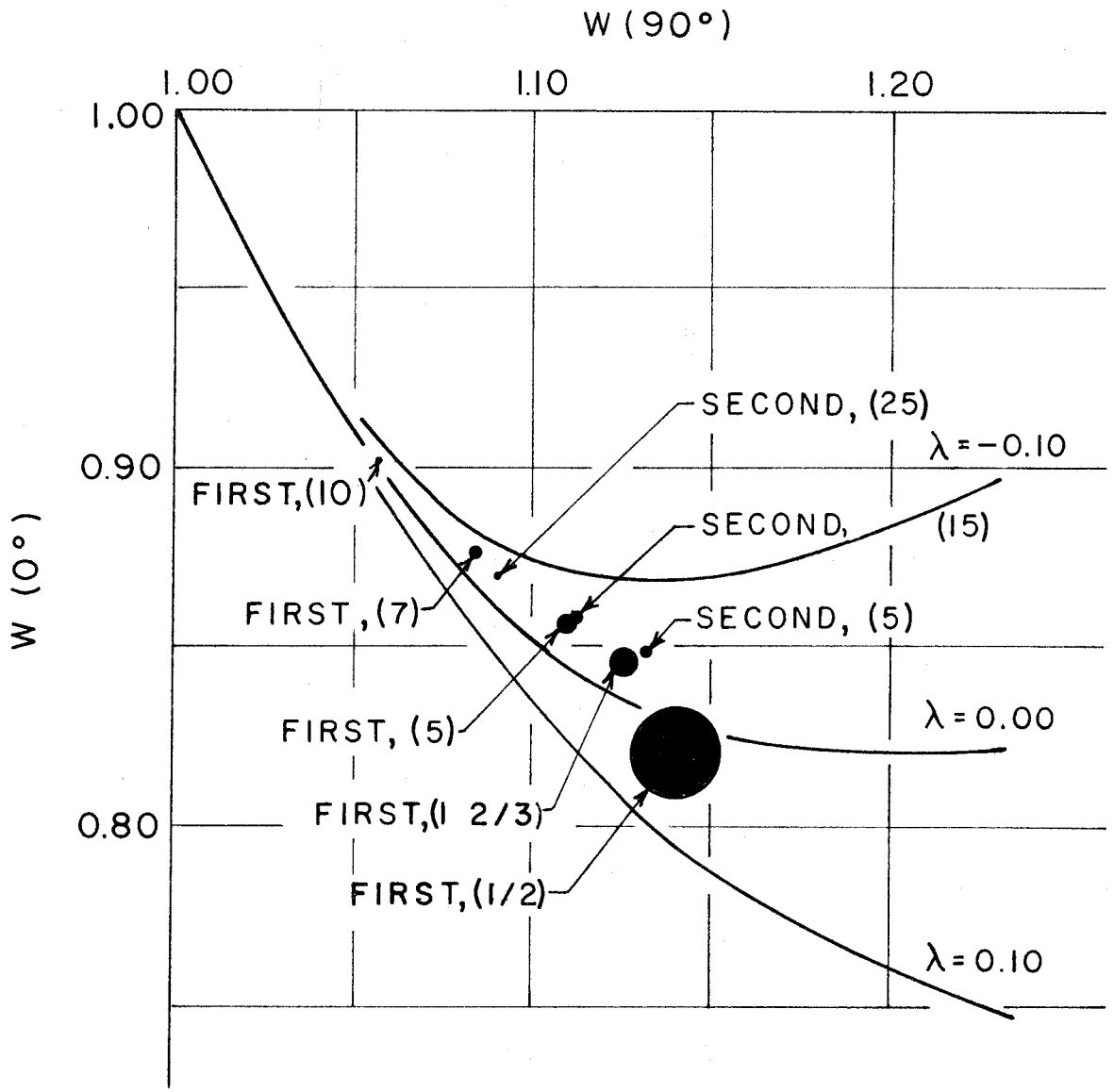

W(0°) VERSUS W(90°) FOR 0% Ni LAYERED CRYSTALS

See caption of figure 6, p. 44.

FIGURE 8

from Oak Ridge contained traces of impurities. When these impurities are concentrated in a thin layer their concentration may be as high as 3/4 molar percent. Some of these impurities are paramagnetic nickel, iron, cobalt, etc. The effect of interactions between the latter two and Co^{58} is unknown.

III.5 4% Ni CRYSTAL

Figure 9 shows the 4% crystal. It is layered, as are the 0% crystals. The crystal weighed 3.5 gms., and contained about 0.7 μcuries of radioactivity. The 4% region of the crystal was in thermal contact with its 12% surroundings through the 0.6 mm layer of 0% material. This material is apparently too poor a thermal conductor to bring about equilibrium between the 4% and the 12% materials in the time of the experiment.*

In this very dilute sample the nickel-nickel interactions are small and the 4% material gets quite cold upon demagnetization (Fig. 10).

III.6 SUMMARY OF RESULTS

Several significant features are apparent in these experimental results:

---

*This is to be expected since the conductivity (K) is

$K \approx 1$ erg/sec-cm-degree (Ref. 30)

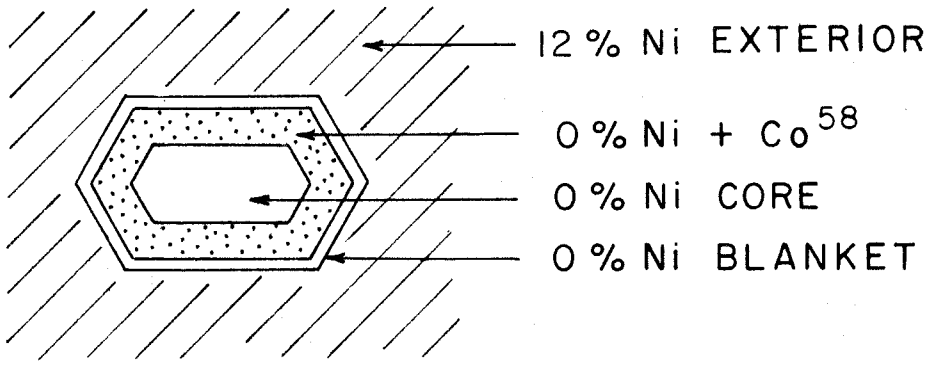

SCALE 10 : 1

STRUCTURE OF 4% Ni CRYSTAL

Cross section perpendicular to the axis of alignment

FIGURE 9

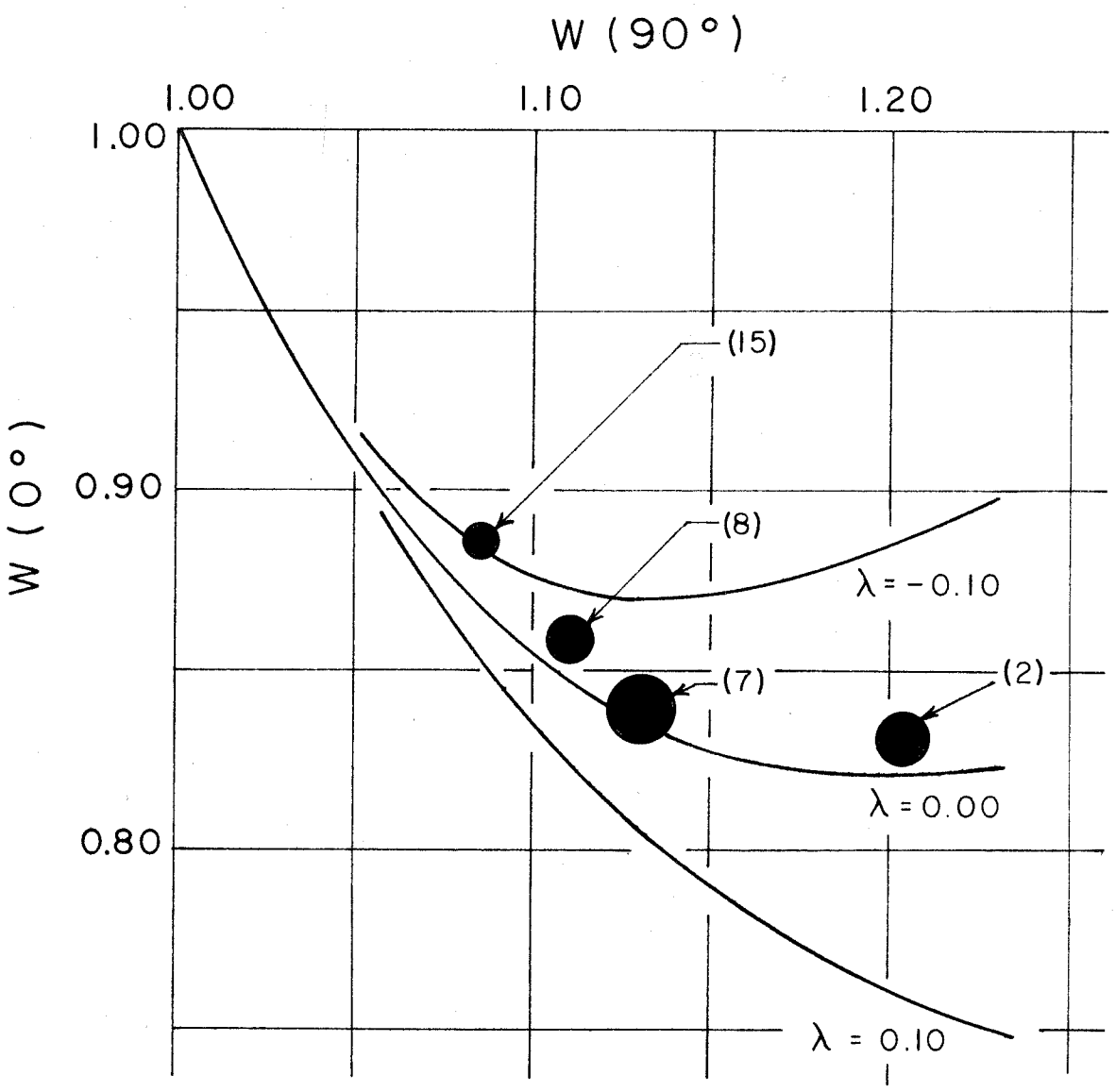

W(0°) VERSUS W(90°) FOR 4% Ni LAYERED CRYSTAL

See caption of figure 6, p. 44.

FIGURE 10

Table 5

Experimental* λ's for 0%, 4%, 6%, 12%, and 19% Ni Crystals

Crystal Temp Range	First 0%	Second 0%	4%	6%	12%	19%
$\beta < 1$	-0.04 ± 0.05	----	----	-0.127 ± 0.01	-0.014 ± 0.015	0.02 ± 0.02
$1 < \beta < 1.3$	-0.06 ± 0.02	-0.052 ± 0.01	-0.11 ± 0.04	-0.102 ± 0.01	-0.043 ± 0.01	----
$1.3 < \beta < 1.6$	-0.04 ± 0.02	-0.054 ± 0.006	-0.04 ± 0.03	-0.064 ± 0.02	----	----
$1.6 < \beta < 2.0$	-0.025 ± 0.02	-0.042 ± 0.004	-0.01 ± 0.03	----	----	----
$2.0 < \beta$	0.02 ± 0.04	----	-0.013 ± 0.008	----	----	----

Values are averages of many demagnetizations grouped into five temperature ranges.

*Fully corrected for the weak competing Co^{58} γ-rays, the finite solid angle of the counters, the measured counter noise, and the contamination of Co^{60} in the sample.

1. The magnitude of λ is generally close to zero, as had been anticipated on the basis of Griffing and Wheatley (Ref. 17), Boehm and Wapstra (Ref. 19), and Dagley et al (Ref. 28).
2. Although close to zero, the measured λ's show a marked dependence on the nickel concentration of the crystal. This concentration dependence greatly exceeds the limits of experimental error.
3. Finally, in a nominal 0% nickel crystal we observe negative λ's.

These behaviorisms provide clues to the mechanisms that are evidently responsible for the discrepancies.

a) On the basis of 2. above we are forced to conclude that the presence of nickel ions in the crystal disturbs the measurement of λ. In some way interactions between the radioactive Co^{58} ions and the nickel ions are affecting the nuclear alignment. This matter is discussed in Section IV.1 to follow.

b) From 3. above we see that even where only small ionic interactions are expected, theoretically "impossible" negative measured λ's are obtained. This consideration reveals that a further mechanism is entering in - a mechanism associated solely with the individual Co^{58} ion. The only likely mechanism is the "K-capture effect". This is discussed in Section IV.2.

The evident inadequacy of the ideal theory for coping with effects thus encountered in actual, experimental systems forces an extension of the theoretical treatment. Resultant modification of theory, and the extent to which these effects thereby become explainable will constitute the remainder of this presentation.

IV. MODIFIED THEORY

The preceding experimental results indicate that the simple ideal theory of Section II is not adequate. As already stated, this theory does not account for the dependence of the measured λ on concentration or for the negative measured λ's in a nominal 0% Ni crystal. The physical problem therefore must be examined much more closely in an effort to understand the discrepancies between such an ideal theory and the observed results. The following presentation will be devoted primarily to the attempts that have been made to provide an adequate theoretical basis for interpreting these results.

IV.1 THEORY INCLUDING INTERACTIONS

a) Introduction

One effect not taken into account by the ideal theory is the matter of ionic interactions. Such phenomena are important in many areas of solid state physics, being for example directly responsible for ferromagnetism and spin-spin relaxation in paramagnetics. Hence it will be of great interest to examine the theory including interactions not only to understand the present experiments, but possibly to shed further light on the properties of magnetic substances in general.

Even a cursory examination of the actual physical situation reveals clearly the inadequacies of the simple

idealized theory. In the crystals generally used in nuclear alignment the radioactive material is in an environment containing an appreciable number of paramagnetic ions. In this case the Hamiltonian equation 20

$$\mathcal{H} = A(S_z I_z) + B(S_x I_x + S_y I_y) \tag{20}$$

which was used to arrive at figure 5 (p. 36) must be modified to become (Ref. 31)

$$\mathcal{H} = A(S_{o,z} I_{o,z}) + B(S_{o,x} I_{o,x} + S_{o,y} I_{o,y}) + \sum_{(ij)} P(\vec{S}_i, \vec{S}_j) + \sum_{i \neq o} D(\vec{S}_i) + \sum_{i \neq o} Q(\vec{S}_i, \vec{I}_i) \tag{30}$$

where

The subscript o denotes the radioactive ion under consideration

the subscript i, or j denotes an arbitrary paramagnetic ion

$P(\vec{S}_i, \vec{S}_j)$ is a function which describes the interaction between paramagnetic ions i, and j

$D(\vec{S}_i)$ is a function of only S_i

$Q(\vec{S}_i, \vec{I}_i)$ describes the hyperfine effects in ion i

$\sum_{(ij)}$ is a sum over all pairs of paramagnetic ions, taking each pair only once.

The energy matrix given by this Hamiltonian is now very large. Instead of 10 x 10 it is n x n where

$$n = (2I_\alpha+1)^{N_\alpha} (2S_\alpha+1)^{N_\alpha} (2I_\beta+1)^{N_\beta} (2S_\beta+1)^{N_\beta} \qquad (31)$$

if there are N_α ions of type α in the crystal and if there are N_β atoms of type β . The problem can no longer be solved exactly even if the P's and Q's are known. However, in the high temperature limit it can be approached with some rigor (Appendix IX). Unfortunately, there is not much information available concerning the P's.

If the P's were associated with magnetic interactions exclusively they would be:

$$P(\vec{S}_i,\vec{S}_j) = \sum_{\alpha\beta} g_{i,\alpha} g_{j,\beta} \beta^2 \left[\frac{\delta_{\alpha\beta}}{r_{ij}^3} - 3 \frac{r_{ij,\alpha} r_{ij,\beta}}{r_{ij}^5} S_{i,\alpha} S_{j,\beta} \right] \qquad (32)$$

where

subscripts and are x, y, and z,

$\delta_{\alpha\beta}$ is Dirac delta function

r_{ij} is the distance between the ions

$r_{ij,\alpha}$ is the length of the projection of this distance on the α axis

$r_{ij,\beta}$ is the length of the projection of this distance on the β axis

$g_{i,\alpha}$ is the g factor in α direction of ion i

$g_{j,\beta}$ is the g factor in the β direction of ion j

is the Bohr magneton

However, exchange effects of the same nature as those responsible for ferromagnetism may be many times as large as the magnetic interactions. The exchange interactions are due to a virtual exchange of electrons between two ions with overlapping wave functions. The exchange is required to symmetrize or antisymmetrize the spatial wave function, depending on whether the intrinsic electron spins are anti-parallel or parallel respectively. The total wave function (space plus spin) must be antisymmetric for an interchange of electrons as required by the Pauli exclusion principle. A good treatment of exchange is given in Van Vleck (Ref. 32).

Because there is little known about these exchange effects, we are forced to guess on scanty evidence at the P terms in $\mathcal{H}$ (Eq. 30). Using this guess we must make a model which will allow us to calculate f_2 and f_4 for Co^{58} from the assumed $\mathcal{H}$. The guess will be used in the following subsections to modify the $W(0^\circ)$ vs. $W(90^\circ)$ curves for Co^{58} (Fig. 5).

b) The static approximation-estimate of the interaction size

Nickel-nickel interactions

Let us consider the physical problem to be solved. The paramagnetic environment of a cobalt ion is made up of nickel ions located at assumedly random zinc ion sites. Consider the nickel ions in detail. From (Ref. 21) and Appendix IV we find that their Hamiltonian is:

$$\mathcal{H}_{Ni}/k = g\beta(H_z S_z + H_x S_x + H_y S_y) + D(S_z^2 - \frac{2}{3}) \qquad (33)$$

where

$$g = 2.3$$

$$D = -0.176^{\circ}K$$

and $$g = 1.55 \times 10^{-4} \text{ degrees/gauss}$$

The effective spin (S') for nickel is 1. No hyperfine splitting has been observed for the 1.25% of the nickel ions with non-zero nuclear spins.

The level structure of nickel in a small magnetic field is as follows:

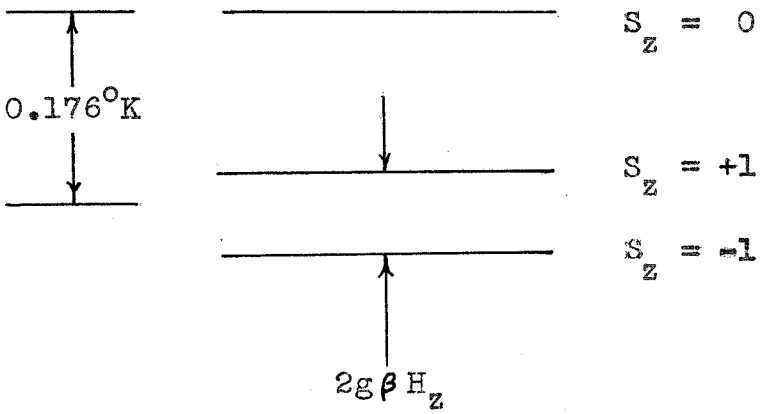

Note that we have neglected mixing of S_z states caused by x or y components of the magnetic field.

Now, if the magnetic field caused by a nearby ion is small, the picture remains the same and we can consider the ions individually. It is meaningful to specify the spin state of a particular ion ($S_z = 0, \pm 1$).

What this means classically is clear--each nickel wants to be pointing in the $\pm$ z direction. To change it from a +z orientation to a -z orientation requires going over a high potential hill at $S_z = 0$. Instead of sharing 1 unit of spin with a nearby nickel (or with all other nickels) and precessing from $S_z = 1$ to $S_z = 0$ and back again as the other nickel does the opposite, it will merely stay in the $S_z = 1$ orientation.

Mathematically, the meaning is that a state described by specifying the z components of angular momentum (S_z) for each of the nickel ions in the crystal is approximately diagonal in the Hamiltonian for the crystal (equation 33 + interaction terms).

The above discussion applies to magnetic dipole couplings and exchange couplings as well. Both are described by interaction terms which look like

$$\sum_{(ij)} \sum_{\alpha\beta} P_{ij,\alpha\beta} \; S_{i,\alpha} S_{j,\beta} \qquad (34)$$

Again i and j are different ions and α and β are x, y, and z.

With this picture for an approximation we can now venture a guess at the <u>size</u> of this interaction from thermodynamic data obtained from demagnetizations. The entropy per ion (S/N) of the nickel ions before and after demagnetization from 0.95° and 22 kilogauss is 0.1 k (Appendix II). We can equate this entropy to the entropy of an ensemble of nickel

ions having the ground state split by energy 2ϵ, again using the static approximation. (Actually 2ϵ is a weighted average of the splittings of all the ions in the crystal--in a dilute crystal each ion sees a somewhat different environment.) Now, since in zero magnetic field, after demagnetization the temperature is about $0.02^{\circ}K$ we can neglect the contribution of the $S_z = 0$ level to the entropy of the crystal. Using figure 15 (p. 94) applying to a three level system with $-D/\epsilon >> 1$, we can see that

$$kT/\epsilon = 0.52 \text{ (for } S = 0.10 \text{ Nk)}. \tag{35}$$

Remembering from equations 29 and 17 (pages 34 and 26)

$$\beta = \frac{A}{2kT} = \frac{0.04}{2kT} \tag{36}$$

or, from equations 35 and 36

$$\epsilon = 0.04/\beta \quad \text{(for } S = 0.10 \text{ Nk)}. \tag{37}$$

Since we know $S = 0.10$ Nk after demagnetization, we can conclude that the lowest temperature obtained in our experiments corresponds to a crystal with $S = 0.10$ Nk. We can use equation 37 to estimate 2ϵ.

Estimates of 2ϵ are given in Table 6 and figure 11. It is emphasized that the values of β thus used to obtain 2ϵ are not obtained from equation 36; rather, they were "apparent β's" deduced from experimental observations with the aid of

the $W(0^{\circ})$ vs. $W(90^{\circ})$ graphs such as figure 5 (p. 36). In other words, these apparent β's are chosen such that when combined with an appropriate λ and using the previous ideal theory they yield the $W(0^{\circ})$ and $W(90^{\circ})$ observed immediately after demagnetization.

Thus, it is directly observable that the effective λ decreases with increasing concentration. By the foregoing analysis this is expressed as an increasing interaction (ϵ) with increasing concentration. Viewed in this manner the ϵ's provide the mechanism to determine the low temperature limit and its concentration dependence.

We have been forced to use the above rather indirect and tenuous procedure for determining ϵ because such direct methods as straight resonance techniques are precluded by the line broadening inherent to such strong interactions.

Nickel-cobalt interactions

Thus we have an idea of the splitting of the nickel ground level. However, we are interested in the splittings of the Co ground level. We must now try to estimate the Co splitting knowing nickel splitting. If the splittings of these ground levels are purely magnetic we expect the average magnitude of the z component of ionic magnetic field* at a

---

*The x and y components of magnetic field will not be very effective in splitting the ground level of the nickel ion because of the large "D" term in the spin Hamiltonian equation 33.

Table 6

Estimates of Nickel-Nickel Ground Level Splittings (2ϵ)
Based on Apparent β's Observed Upon Demagnetization

Crystal	β	$2\epsilon = \frac{0.08}{\beta}$ (in degrees)
4% Ni	3.4 ± 0.5	0.024 ± 0.004
6% Ni	1.35 ± 0.13	0.060 ± 0.009
12% Ni	1.35 ± 0.13	0.060 ± 0.009
19% Ni	1.05 ± 0.10	0.072 ± 0.012

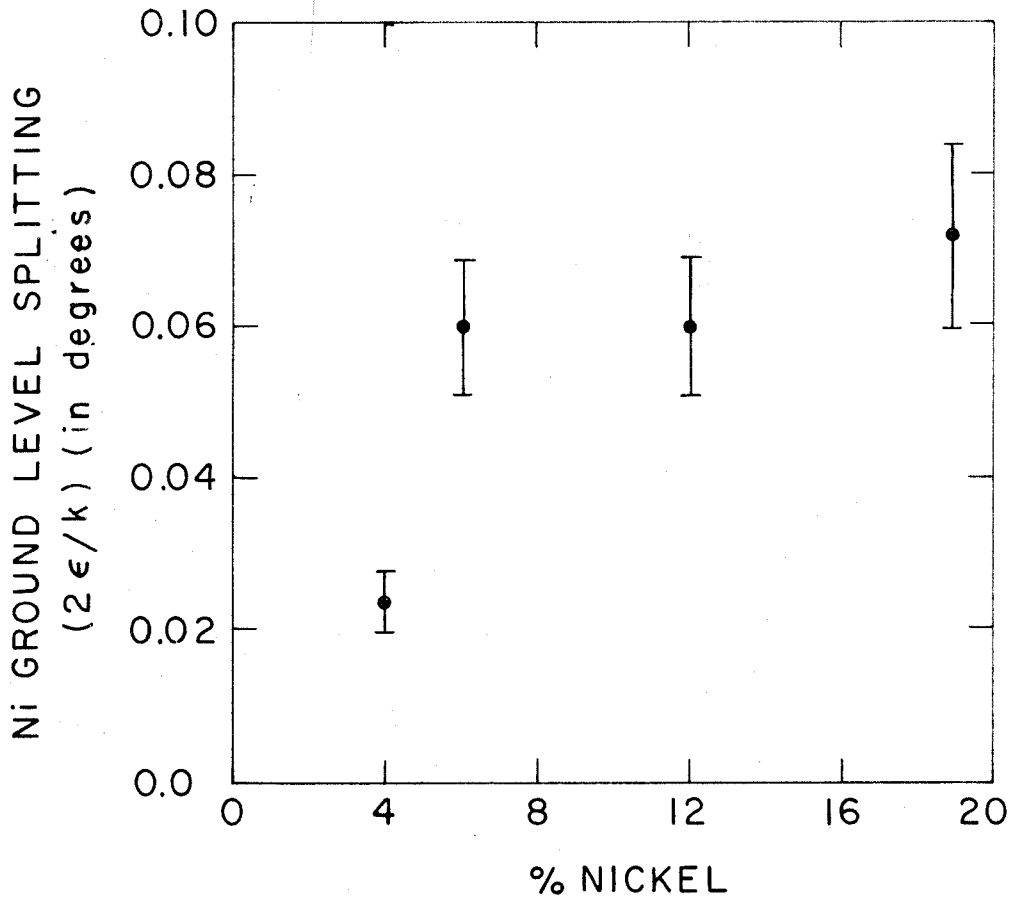

ESTIMATES OF GROUND LEVEL SPLITTINGS (2ϵ)

OF NICKEL IONS IN $(Ni,Zn)SiF_6 \cdot 6H_2O$

Based on apparent temperatures obtained upon demagnitization. See text.

FIGURE 11

Ni ion site in a 6% Ni crystal to be, from equation 33 (p. 57) and figure 6 (p. 44):

$$H_z = \frac{2\epsilon}{(1.55 \times 10^{-4})\Delta S_z} = 200 \text{ gauss} \qquad (38)$$

$\Delta S_z = 2$ = the difference between S_z in the two ground states.

on the basis of the present observations.

By using this field in equation 17 (p. 26) we can obtain an estimate of the effect of the z directed ionic field on the spin Hamiltonian for cobalt. This leads to a splitting of the electronic ground state of:

$$2\epsilon\big|_{Co} = 3.91 \times 10^{-4} \times 200 \times 1 = 0.078 \text{ k} \qquad (39)$$

On the other hand, suppose that the principal cause of the nickel and cobalt ground level splittings is electron exchange. Then it becomes more difficult to guess at the cobalt-nickel interactions. We know that the cause of exchange forces is an overlap of the electronic wave functions of two nearby ions. It is reasonable to expect that the overlap (and most likely the exchange energy) of a cobalt-nickel pair will be between that of a cobalt-cobalt pair and a nickel-nickel pair. Fortunately there is some evidence concerning the cobalt-cobalt and nickel-nickel interactions.

Appendix X reviews this data and concludes that cobalt-cobalt exchange energy is about 7 times that of nickel-nickel

exchange. Hence, we may expect the cobalt-nickel interaction to be about 2.5 times that of the nickel-nickel interaction.*

On this basis we may expect splittings of the electronic level of cobalt to be

$$2\epsilon\Big|_{Co} = 2.5 \times 2\epsilon\Big|_{Ni} \tag{40}$$

In a 6% Ni crystal $2\epsilon\Big|_{Ni}$ is about 0.06 k (Fig. 11). In that case

$$2\epsilon\Big|_{Co} = 0.15 \text{ k} \tag{41}$$

Hence, the static picture can be expected to bear some semblance to reality since the interactions, while not small, are less than the "D" term in equation 33 which elevates the $S_z = 0$ level. Calculations based on the static model do tend to agree with experiment, and will be discussed in the following subsection.

c) The static approximation--Results

In the static approximation the Co^{58} electrons are coupled by a magnetic field, or an effective magnetic field due to exchange effects to fixed magnetic nickel ions. Equation 16 (p. 25) can be written as:

$$\mathcal{H}/k = G_z S_z + G_x S_x + G_y S_y + A S_z I_z + B(S_x I_x + S_y I_y) \tag{42}$$

*By a quantum mechanical argument based on the relative size of wave functions the interaction between unlike species may be seen to be roughly the geometric mean of the associated functions for like species.

for convenience change to energy units of 0.04 k.

$$\mathcal{H} = G_z S_z + G_x S_x + G_y S_y + S_z I_z + B(S_x I_x + S_y I_y) \qquad (42a)$$

where all the quantities G_z, G_x, G_y, B and $\mathcal{H}$ are in units of A = 0.04 k. This simplification results in the coefficient unity for the coefficient of the $S_z I_z$ term.

And

$$B/A = \frac{1}{4} \qquad (42b)$$

$$G_z = \frac{0.078}{0.04} \text{ to } \frac{0.15}{0.04}$$

$$= 2 \text{ to } 4$$

from equations 39 and 41.

Each Co^{58} ion will have a different value of G_x and G_y. Since there is axial symmetry averaged over all ions we need only compute the population distribution functions f_2 and f_4.* These two numbers along with a known decay scheme completely describe an axially symmetric angular distribution of quadrupole γ-rays. We set $G_y = 0$ and compute the statistical average of I_z^2 and I_z^4 for a given positive value of G_x (and G_z). Clearly by the symmetry of the Hamiltonian these statistical averages are unchanged for the same negative values of G_x or for the same positive or negative value of G_y (when $G_x = 0$). Of course, changing the sign of G_z has no effect because we are computing only the even moments of the nuclear spin.

---

*If there is a net polarization of the crystal this is not true.

Setting $G_y = 0$ and using the techniques of Section II.3 the energy determinate of equation 42a becomes:

(See Page 67)

This cannot be diagonalized manually. However, it was diagonalized on the Datatron 205* for several values of the variables G_x and G_z. Proceeding exactly as in Section II.4 we arrive at $W(0^\circ)$ and $W(90^\circ)$ for $\beta = 1$, 1.5, and ∞ for different choices of the variables (Table 7). Some of the W's are plotted in figure 12.

IV.2 K-CAPTURE DEALIGNMENT

a) The problem

Another inadequacy of the ideal theory for coping with the complications of systems experimentally encountered results from the complete neglect of dealignment processes occurring within the ion itself. For example, the 84% of nuclei undergoing K-capture are subjected to strong precessional effects during the short lived interval following β-decay and preceding γ-emission. Such precession is produced by magnetic interactions with the electronic shell. Since very little is known concerning such processes the following discussion will be highly speculative.

We will be primarily concerned with the effects of reorientation on the 84% of the nuclei which K-capture. For

---

*Program Code 2.42.025 by Christopher and H. Fox was used.

S_z, I_z	$\frac{1}{2},2$	$-\frac{1}{2},2$	$+\frac{1}{2},1$	$-\frac{1}{2},1$	$+\frac{1}{2},0$	$-\frac{1}{2},0$	$+\frac{1}{2},-1$	$-\frac{1}{2},-1$	$+\frac{1}{2},-2$	$-\frac{1}{2},-2$
$\frac{1}{2},2$	$\frac{G_z}{2}+1-E$	$\frac{G_x}{2}$								
$-\frac{1}{2},2$	$\frac{G_x}{2}$	$-\frac{G_z}{2}-1-E$	B							
$+\frac{1}{2},1$		B	$\frac{G_z}{2}+\frac{1}{2}-E$	$\frac{G_x}{2}$						
$-\frac{1}{2},1$			$\frac{G_x}{2}$	$-\frac{G_z}{2}-\frac{1}{2}-E$	$\frac{6B}{2}$					
$+\frac{1}{2},0$				$\frac{6B}{2}$	$\frac{G_z}{2}-E$	$\frac{G_x}{2}$				
$-\frac{1}{2},0$					$\frac{G_x}{2}$	$-\frac{G_z}{2}-E$	$\frac{6B}{2}$			
$+\frac{1}{2},-1$						$\frac{6B}{2}$	$\frac{G_z}{2}-\frac{1}{2}-E$	$\frac{G_x}{2}$		
$-\frac{1}{2},-1$							$\frac{G_x}{2}$	$\frac{G_z}{2}+\frac{1}{2}-E$	B	
$+\frac{1}{2},-2$								B	$\frac{G_z}{2}-1-E$	$\frac{G_x}{2}$
$-\frac{1}{2},-2$									$\frac{G_x}{2}$	$-\frac{G_z}{2}+1-E$

Table 7

Theoretical $W(0^\circ)$ and $W(90^\circ)$ with Static Interactions (K-capture not included)

G_x \ G_z	0.4	0.6	0.8	1.2	2.8
0.4		14 .8822 1.0723 .8415 1.1162 .8263 1.2392 -- --			
0.6	11 .8865 1.0696 .8486 1.1100 .8231 1.2337 -- --		19 .8838 1.0713 .8421 1.1154 .8262 1.2389 -- --		
0.8	12 .8907 1.0669 .8524 1.1048 .8208 1.2293 -- --	16 .8892 1.0678 .8506 1.1080 .8229 1.2332 -- --			
1.2				3 .8914 1.0659 .8481 1.1086 .8228 1.2340 -- --	2 .8757 1.0744 .8308 1.1246 .8293 1.2440 -- --
2.8				4 .9273 1.0430 .8940 1.0703 .8053 1.1952 .8490 1.1192	1 .9015 1.0594 .8540 1.1016 .8199 1.2290 -- --

$\lambda = 0$; G_z and G_x are in energy units of $A = 0.04$ k. The numbers given above are arranged in the arrays as follows:

Case No.

$W(0^\circ)_{\beta=1}$ $W(90^\circ)_{\beta=1}$

$W(0^\circ)_{\beta=1.5}$ $W(90^\circ)_{\beta=1.5}$

$W(0^\circ)_{\beta=\infty}$ $W(90^\circ)_{\beta=\infty}$

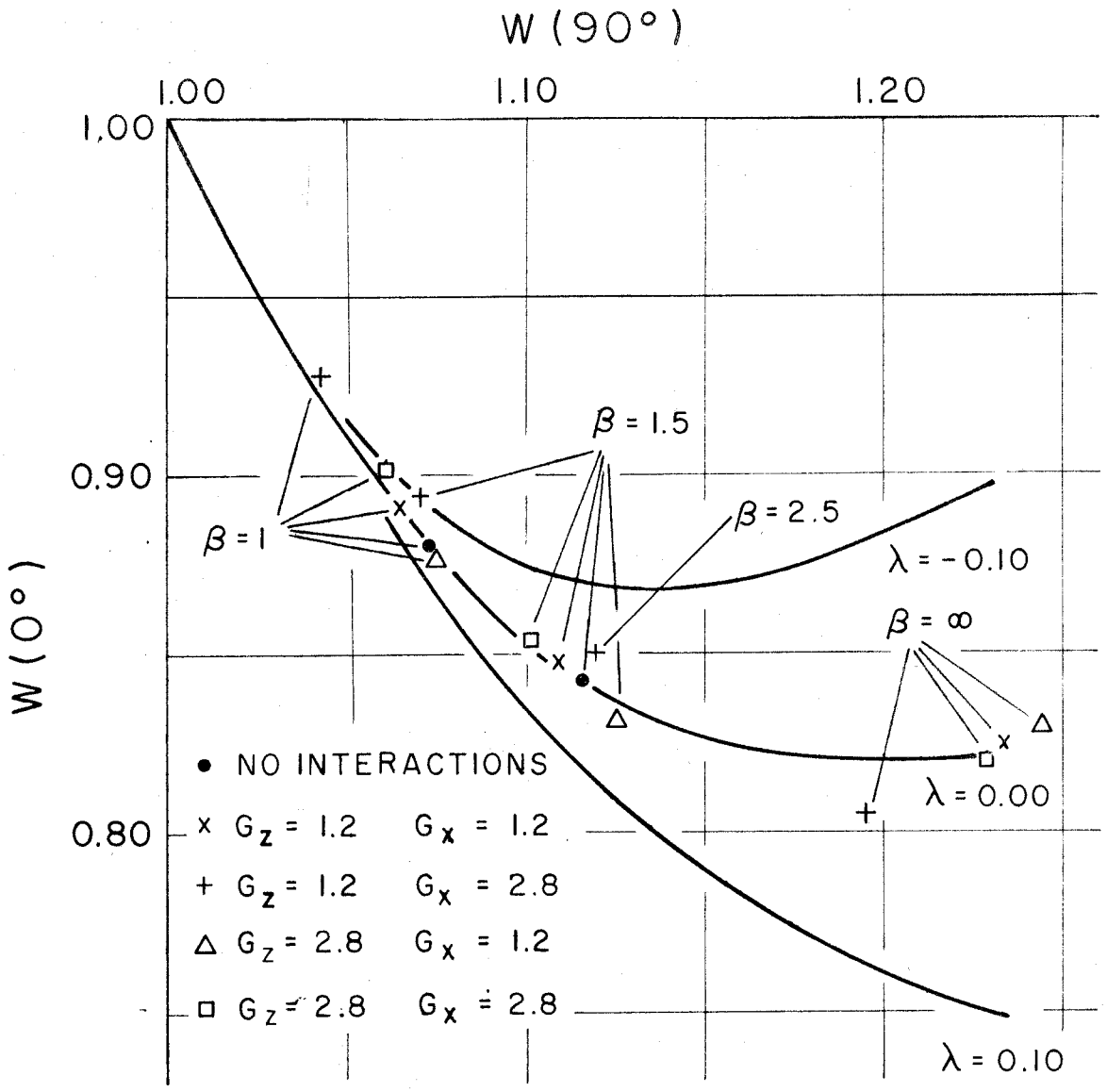

THEORETICAL COUNTING RATES W(0°) AND W(90°) WITH STATIC INTERACTIONS AND $\lambda = 0$

G_z and G_x are in units of A = 0.04 k .

Curves are for ideal theory (Fig. 5) .

Note the large effect of interactions in the case G_z = 1.2 and G_x = 2.8 .

FIGURE 12

about 3.8×10^{-16} seconds* the K-shell hasonly one electron and the coupling between this electron and the nucleus is huge. Fermi (Ref. 34) shows that the energy splitting (ΔE) between the F = 5/2 and F = 3/2 states of the system (spin 2 nucleus plus electron) is given by

$$\Delta E = \frac{8\pi}{3} \left(\frac{2I + 1}{I}\right)\left(\mu_N \beta\right)\left|\psi(0)\right|^2 \qquad (44)$$

where

μ_N is the nuclear magnetic moment

β is the Bohr magneton

I is the nuclear spin

$\psi(0)$ is the wave function of the K electron at the nucleus.

Using a hydrogen-like wave function with Z = 26 for this innermost electron and if we use $g_N = 0.4$ (see page 86) as the nuclear g-factor of this intermediate state we find that:

$$\Delta E = 0.019 \text{ ev} \qquad (45)$$

---

*This mean time (τ') before an electron from an outer shell drops into a K-shell vacancy is readily ascertained. The K_{α_1} x-ray line width is 2.5 ev and the K_{α_2} is 2.6 ev (Ref. 33). If we take the width of the L-shell to be 1/4 of the line width we get the K-shell width as 0.75 x 2.5 ev or 1.75 ev. We get the life time of the state to be

$$\tau' = \frac{\hbar}{1.75 \text{ ev}} = \frac{6.6 \times 10^{-16} \text{ ev sec}}{1.75 \text{ ev}}$$

$$= 3.8 \times 10^{-16} \text{ sec}$$

However, relations given in Subsections b) and c) can be used to show that even with this large coupling, the lifetime of the state (τ') is too small by a factor of 50 to give appreciable nuclear realignment.

After the K-capture there is a rapid cascade as electrons fall from higher energy levels into lower vacant levels. Sometimes an x-ray is emitted as an electron falls, but more often the energy is conserved in the cascade by ejecting a less strongly bound electron from the ion (Auger effect). After this cascade, which lasts about 10^{-14} seconds, the ion is left highly ionized (Ref. 35) and optically excited. (Optical transitions take about 10^{-8} seconds; the γ-emission takes place in a much shorter time.)

It takes about 25×10^{-12} seconds* for the γ-ray to be

---

*We are interested in a 810 kev γ-transition going from a 2+ level to a 0+ level in $_{26}Fe^{58}$ (see Fig. 1, p. 4). While the mean life (τ) of this nuclear level in Fe^{58} is not known the half-life ($t_{1/2}$) of the 2+ level in Fe^{56} is 6.0×10^{-12} sec, in $_{28}Ni^{60}$ it is greater than 3×10^{-12} sec, and in $_{30}Zn^{64}$ it is 2.6×10^{-12} sec (Ref. 36). All these are even-even nuclei and the decay is to the 0+ ground state. We may expect the corresponding Fe^{58} level to have the same lifetime, except for an E^5 energy dependence. Extrapolating to 810 kev using the E^5 law we find the following estimates for the half-life of the excited state of Fe^{58}

$$t_{1/2}|_{Fe^{58}} = 7 \times 10^{-12} \text{ sec extrapolated from } Fe^{56}$$
$$> 36 \times 10^{-12} \text{ sec extrapolated from } Ni^{60}$$
$$= 7 \times 10^{-12} \text{ sec extrapolated from } Zn^{64}$$

Taking an average of these estimates we find that

$$t_{1/2}|_{Fe^{58}} \approx 17 \times 10^{-12} \text{ sec}$$

or

$$\tau|_{Fe^{58}} = t_{1/2}/.69 = 25 \times 10^{-12} \text{ sec}$$

probably to within a factor of 2.

emitted after the nucleus has K-captured. It is during this time that we expect nuclear dealignment to take place.

It is difficult to treat dealignment in this state accurately. The reason is clear. Before the K-capture the electronic shell as well as the nucleus is aligned. After the K-capture and the Auger effect has taken place the electron shell (and of course the nucleus) will "remember" their initial alignment to a certain extent.

As a matter of fact, the wave function of the lowest energy states before the K-capture has the paramagnetic electron pointed opposite to the nucleus since A in the spin Hamiltonian (Eq. 20, p. 27) is positive. Thus in the most populous states the z component of spin of the total system (electron plus nucleus) is 1/2 smaller in magnitude than the nuclear spin magnetic quantum number (I_z). During the precession following the K-capture and the Auger effect, if the electronic shell remembers this initial situation, the system will precess between from the $|I_z, -1/2\rangle$ and $|I_z\ -1, 1/2\rangle$ state and back again (I_z taken as positive). This is a dealignment of the nucleus. This effect is considered by Steenburg (Ref. 37) and his conclusions are given in Subsection c).

However, there are reasons why the electronic shell may not remember its initial alignment too well. On the average there are four particles given off during and after the K-capture.

There is one neutrino, about three Auger electrons (Ref. 35), and an occasional x-ray; each of these carries at least 1/2 unit of angular momentum from the system. Thus during the time following the Auger cascade the electronic shell is losing some of its initial orientation.* The dealignment effect of an unoriented shell is discussed in Subsection b).

b) Theory of reorientation with an isotropic electron shell of spin = 1/2

If, after the Auger effect the electronic shell is in a spin 1/2 state and is spherically symmetric i.e., it is unpolarized and has the spin Hamiltonian:**

$$\mathcal{H} = A^i \quad (\vec{S}^i \cdot \vec{I}^i) \tag{46}$$

then the effect of reorientation is easy to work out. This has been done by Tolhoek et al (Ref. 38) and they find that

$$W(\theta) = 1 - \frac{5}{7}(1 + \lambda)\, f_2 Q_2 P_2(\cos\theta) + \frac{80}{9}(1 - 2.5\lambda)\, f_4 Q_4 P_4(\cos\theta) \tag{47}$$

---

*As an added complication, we must remember that these particles are not given off randomly; for example, the neutrino which is emitted by a polarized nucleus is itself polarized. Similarly, the Auger electrons which result from a cascade between polarized electronic sub-shells are polarized. Hence, while the K-capture, and the following cascade would have a tendency to dealign the aligned electron shell, they will also have a tendency to realign it. More rigorous attempts to understand K-capture dealignment have also been doomed to failure because of the complexity of the problem.

**The i's are to denote that these are quantities relating to the intermediate state.

where

λ is the usual β-decay parameter

$f_{2,4}$ are the alignment parameters of the initial Co^{58} state

$Q_{2,4}$ are attenuation parameters associated with the nuclear precession in the intermediate state

$$Q_2 = 1 - 0.24\,\Delta \tag{48a}$$

$$Q_4 = 1 - 0.80\,\Delta \tag{48b}$$

where, if the state has mean life τ :

$$\Delta = \frac{(5\alpha)^2}{1 + (5\alpha)^2} \tag{49}$$

and

$$\alpha = \frac{A^i \tau}{2\hbar} \tag{50}$$

/The reason for this somewhat devious definition of α is that it is the important quantity in the Subsection c). The energy difference (ΔE) between the F = 5/2 and F = 3/2 state of the coupled electron and nucleus system is $5A^i/2$ (Eq. 14 of Ref. 14)./

The effect of this type of reorientations is given in figure 13 for the exemplary case of $\alpha^2 = 0.02$. We have assumed that $\lambda = 0$, and that f_2 and f_4 are given by the non-interacting theory. It should be mentioned that the effect of realignment on $W(0^\circ)$ and $W(90^\circ)$ is proportional to Δ as

can be seen by substituting equations 48a and 48b into equation 47. Δ is roughly proportional to α^2 in region of $\alpha = 0.14$.

Thus, with a spherically symmetric electron shell and an α of 0.14 the effect on the observed λ is not large. It moves the λ in the positive direction about 0.03--opposite to that observed with the 0% Ni crystal.

c) Theory of reorientation where the electronic shell "remembers" its initial alignment

If the alignment of the electron shell after K-capture and Auger effect is the same as before, and if it has spin 1/2 the work of Steenberg allows us to compute the effect of realignment on the angular distribution.

He gives the changes in the intermediate state populations, $\Delta a_{I_z^i}$, as a power series in $A/2kT = \beta$. (We are adapting his notation to that used by Cox and Tolhoek.) By using the definitions of these alignment parameters in terms of the intermediate state populations (Eq. 8a and 8b, pp. 19 and 20) we can arrive at values for the changes in the alignment parameters (Δf_2^i and Δf_4^i) in terms of changes in the intermediate state populations.

If the spin Hamiltonians for the initial and intermediate states are respectively

$$\mathcal{H} = AS_zI_z + \frac{1}{4}A(S_xI_x + S_yI_y) \qquad (51a)$$

$$\mathcal{H} = A^i S_z^i I_z^i + B^i(S_x^i I_x^i + S_y^i I_y^i) \qquad (51b)$$

then we find

$$\Delta f_2^i = \alpha^2(B_1\beta + B_2\beta^2)\, D_2(\alpha^2) \tag{52a}$$

$$\Delta f_4^i = \alpha^2(B_1\beta + B_2\beta^2)\, D_4(\alpha^2) \tag{52b}$$

where

$$B_1 = \frac{1}{6}\, x^i(x^i - 0.25) \tag{53a}$$

$$B_4 = 0.052(x^i)(x^i - 0.4) \tag{53b}$$

with

$$x^i = B^i/A^i \tag{53c}$$

Now for small α^2:

$$D_2(\alpha^2) = -21 \tag{53d}$$

$$D_4(\alpha^2) = 0 \tag{53e}$$

We now know Δf_2^i and Δf_4^i as a function of α^2, x^i, and temperature. From equations 10a and 12a (pp. 20 and 21) we see that

$$W(\theta) = 1 - \frac{10}{7}\, f_2^i\, P_2(\cos\theta) - \frac{40}{3}\, f_4^i\, P_4^i(\cos\theta) \tag{54}$$

hence the change in $W(\theta)$ due to precession in the intermediate state is:

$$\Delta W(\theta) = -\frac{10}{7}\Delta f_2^i\, P_2(\cos\theta) - \frac{40}{3}\Delta f_4^i\, P_4(\cos\theta) \tag{55}$$

where Δf_2^i and Δf_4^i are obtained from equations 52a and 52b.

This effect is shown in figure 13.

When α^2 is not small, $D_2(\alpha^2)$ and $D_4(\alpha^2)$ become:

If $x^i = B^i/A^i = 1$

$$D_2(\alpha^2) = -\frac{21}{1 + 25\alpha^2} \tag{56a}$$

$$D_4(\alpha^2) = 0 \tag{56b}$$

If $x^i = 1.41$

$$D_2(\alpha^2) = -21(1 - 42\alpha^2 + \ldots\alpha^4 + \ldots \tag{57a}$$

$$D_4(\alpha^2) = -20(\alpha^2 + \ldots\alpha^4 + \ldots \tag{57b}$$

If $x^i = 0.5$

$$D_2(\alpha^2) = -21(1 - 12\alpha^2 + \ldots \tag{58a}$$

$$D_4(\alpha^2) = 15(\alpha^2 + \ldots \tag{58b}$$

If $x^i = 0$

$$D_2(\alpha^2) = -21(1 - 8\alpha^2 + \ldots \tag{59a}$$

$$D_4(\alpha^2) = 20(\alpha^2 + \ldots \tag{59b}$$

Figure 13 shows the effect of a gross variation of x^i on the direction in which a theoretical point is moved on the $W(0^\circ)$ vs. $W(90^\circ)$ graph if we take α^2 as 0.02. The distance that a point is moved on this graph is given for $(B_1\beta + B_2\beta^2) = 0.04$. This quantity is very sensitive to variations in x^i

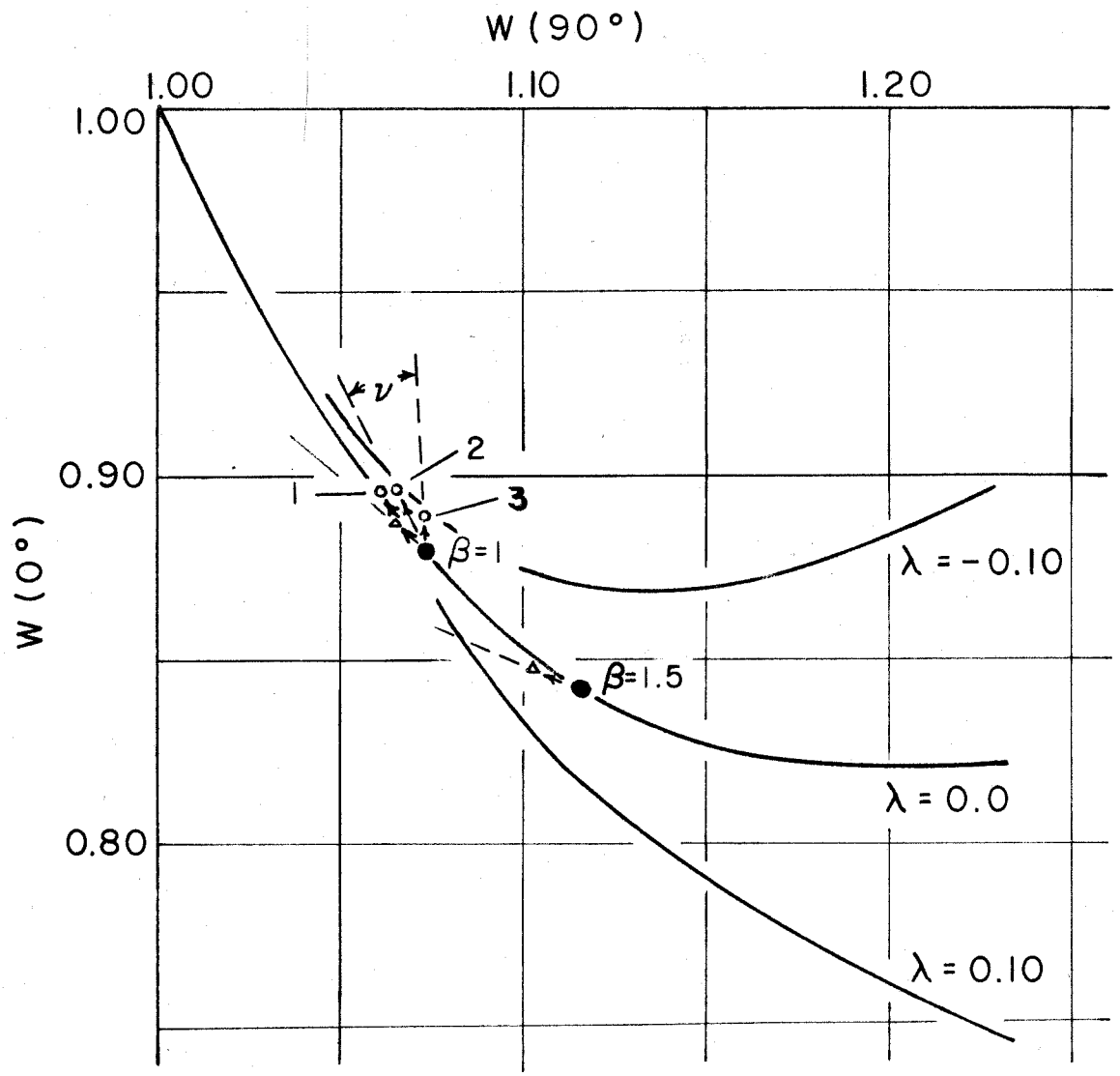

CALCULATION OF K-CAPTURE DEALIGNMENT OF THE INTERMEDIATE STATE (i) ON W(0°) AND W(90°) (In Absence of Ionic Interactions)

Solid lines and solid circles (● ——) computed for ideal theory (no K-capture dealignment, i.e., $\alpha^2 = 0$). β-values as indicated.

Open circles and triangles (○, △) computed for K-capture dealignment, for the case $\lambda = 0$, and $\alpha^2 = (A^i\tau/2\hbar)^2 = 0.02$. Arrows indicate resultant relocation (same β's).

Dealigned Shell (Sec. b)	Aligned Shell (Sec. c)
($x^i = B^i/A^i = 1$)	(1) $x^i = 0$, (2) $x^i = 0.5$ and 1.0, (3) $x^i = 1.41$

FIGURE 13

(see Eq. 53a and 53b). Note that if we hold x^i and α^2 approximately constant and double the value of $(B_1\beta + B_2\beta^2)$ we also double the distance that a point is moved, but do not appreciably change its direction. Also, it can be shown that if α^2 is decreased by a factor of 2 the angle (ν) for any value of x^i (see Fig. 13) is cut approximately in half. If α^2 is increased by a factor of 2 then ν is about doubled.

We now mention that we have not included the effect of a magnetic field on the K-capture dealignment. For small axial fields and small values of α^2 (i.e., $\alpha^2 \lesssim 0.02$ and $G_z^i/A^i \lesssim 1$* Steenberg power series expansion shows no effect). However, for large values of G_z^i/A^i we expect that the electron will precess so rapidly around the z axis that the off axis components of its field at the nucleus will average out to zero in the time that it takes for the nucleus to precess around the electron's field. The z-component of the electron's field will not dealign the nucleus, and we expect no K-capture dealignment.

---

*G_z is the standard notation of equation 16, p. 25.

V. INTERPRETATION

V.1 IONIC INTERACTIONS

These experiments indicate the presence of both K-capture dealignment in the intermediate state and perturbations of the initial nuclear alignment due to ionic interactions. As an approximation to reality we shall for the most part discuss these two phenomenon and their effects on the angular distribution as if they were independent.

Under the above assumptions we can determine the effect of ionic interactions on the measured λ. If interactions are not important in the nominal 0% Ni crystals, then any difference ($\Delta\lambda_{\text{Ionic}}$) between the measured λ's of a 0% Ni crystal and another crystal must be due to interactions. Any non-interaction effects are included in the measured λ of the 0% Ni crystal. $\Delta\lambda_{\text{Ionic}}$ is merely the λ of a given crystal at a given temperature, minus the measured λ of the 0% crystal at the same temperature. This difference has been tabulated in Table 8 where we have used the weighted average of the two 0% crystals for the λ of a 0% crystal.

The first thing that becomes apparent from this table is that the ionic interactions have their greatest effect on the experimental λ's in the higher temperature regions. From figure 12 (p. 69) we see that the static model of Section IV.1 predicts this. Suppose for example that $G_z = 1.2$ and $G_x = 2.8$ with the apparent β about 1. The real β (i.e., $A/2kT$) is about 1.5 and we would expect to measure a λ

Table 8

Values of Observed Change ($\Delta\lambda_{Ionic}$) in Measured λ Attributable to Ionic Interactions

Temp. Range \ Crystal	4%	6%	12%	19%
$\beta < 1$	----	$- 0.09 \pm 0.05$	$+ 0.03 \pm 0.05$	$+ 0.06 \pm 0.05$
$1 < \beta < 1.3$	$- 0.06 \pm 0.04$	$- 0.05 \pm 0.01$	$+ 0.01 \pm 0.01$	----
$1.3 < \beta < 1.6$	$+ 0.01 \pm 0.03$	$- 0.01 \pm 0.02$	----	----
$1.6 < \beta < 2.0$	$+ 0.03 \pm 0.03$	----	----	----
$2.0 < \beta$	$- 0.03 \pm 0.04$	----	----	----

The values in the above table were obtained by taking the difference between the experimentally measured λ of a particular crystal at a particular temperature and the weighted average of the two 0% Ni crystals. Thus, $\Delta\lambda_{Ionic}$ represents the experimentally observed change in the measured λ brought about by the presence of ionic interactions.

of about 0.10 less than the true λ. Whereas if the apparent β is about 1.5 then we expect a discrepancy of only 0.03 in λ.

In a 12% Ni crystal the experimental results are not greatly influenced by the presence of ionic interactions. Below this point $\Delta\lambda_{Ionic}$ is negative while above this point it is positive. Apparently the reason for this is that below 12% Ni there are not enough paramagnetic ions to make the x and y components of the electronic coupling (G_x, and G_y in equation 42) small because of averaging over many ions. The natural symmetry of the crystal is not effective. As a result the coupling constants G_x and G_y are slightly greater than G_z (see Fig. 12).

But, for concentrations above 12% Ni this is no longer true. The G_z fields have gotten larger because of the greater ionic concentration, while G_x and G_y have not grown as fast, if they have grown at all. G_x and G_y are less than G_z and the ionic effect is to make $\Delta\lambda_{Ionic} > 0$.

However, it is not easy to see why $\Delta\lambda_{Ionic}$ is so large ($\Delta\lambda_{Ionic} = 0.06 \pm 0.05$). The choices of G_x and G_z made in Table 7 (p. 68) do not give such large λ's. Attempts to find a choice of G_x and G_z which gives λ's of this size have failed.

The cause of a poor understanding of the 19% Ni crystal may lie in the inadequacy of the theory to handle intermediate state dealignment in the presence of large magnetic fields - G_z/A is 2 to 4 from equation 42b.

V.2 THE K-CAPTURE EFFECT

A modified theory based on ionic interactions alone is not sufficient to explain all of the experimental results - i.e., it fails to explain the appearance of negative λ's in the case of the 0% nickel crystals. Clearly some other mechanism is contributing. This must be a mechanism associated with individual Co^{58} ions themselves.

The mechanism which seems most likely* is associated with the dialignment of the nucleus during the roughly 2×10^{-11} seconds following K-capture and preceding γ-emission. During this time the nucleus precesses due to its magnetic coupling to the electronic shell.** The accuracy of experiments in crystals which are comparatively free of paramagnetic ions makes it possible to detect very small precessions.

Section IV.2 attempts to theoretically analyze the situation in two different cases under two different simplifying assumptions: first, that the electronic shell is dealigned and spherically symmetric during the 2×10^{-11} seconds following K-capture and second, that the electronic shell maintains the same polarization that it had before the K-capture. The theoretical results are shown in figure 13, page 78, where the effect on the measured λ due to K-capture

---

*Other possibilities are discussed and rejected in the footnote on page 99 .

**This coupling, in terms of an effective electronic magnetic field at the nucleus is typically 10^5 to 10^6 gauss in paramagnetic ions.

is shown. The effect predicts a displacement of the $W(0^{o})$ and $W(90^{o})$ observations - graphically illustrated for Co^{58} with a true λ of zero, and which is unaffected by ionic interactions.

From the experimental results of our 0% Ni crystals we are led to the conclusion that the effect on the intermediate state of nuclear reorientation is to yield a more negative measured λ. Figure 13 demonstrates that this is not consistent with a picture of a spherically symmetric electron shell which completely forgets its initial alignment after K-capture and Auger effect - i.e., a dealigned shell. However, it is consistent with an electronic shell which completely remembers its initial alignment after the neutrino and three Auger electrons have left the ion. What actually happens is something in between. However, it is clear from figure 13 that for a given small precession angle α, the "shell which forgets" has smaller effect on the measurement of λ then "the shell which remembers" (except if $x^{i} \sim 0$). This can be seen from the fact that the triangular point for $\beta = 1$ in figure 13 has a λ of about + 0.03 while points 2 and 3 have λ's of about -0.07.

Thus, since there is probably a little of each effect present it is not unreasonable to expect negative λ's in the 0% crystal on the basis of the above very sketchy picture.

However, even at this point we can do some interesting speculation. Suppose we examine figure 13. If we let $x^i = B^i/A^i = 1$ and $\beta \approx 1$ then $(B_1\beta + B_2\beta^2) \approx 0.10$. If $\alpha^2 = 0.005$ we get a measured λ which is about -0.04 as observed. Here we have assumed that the real nuclear λ is zero. If the real nuclear λ is +0.04, then all values of α^2 in the following discussion must be doubled.*

Suppose that we attenuate the theoretical K-capture effect due to "a shell that remembers" by an arbitrary factor of 4 to allow for the fact that it only partially remembers. Then $\alpha^2 = 0.005 \times 4 = 0.02$ is consistent with experiment.

Under the above assumptions, then, we see that

$$\alpha = .14 = \frac{A' \tau}{2\hbar} \tag{60}$$

or

$$A^i = \frac{2\alpha\hbar}{\tau} \tag{60a}$$

Now if the lifetime of the intermediate state (τ) is 25×10^{-12} seconds (p. 71)

$$A^i = \frac{2(0.14)(1.05 \times 10^{-27})}{25 \times 10^{-12}} \text{ ergs} \tag{61}$$

$$= 0.12 \times 10^{-16} \text{ ergs}$$

$$A^i/k = \frac{0.12 \times 10^{-16}}{1.4 \times 10^{-16}} = 0.08^{\circ}K \tag{61a}$$

---

*If λ were known to be zero, it would be possible to deduce a value for the quantity $(\Delta\lambda)_{\text{K-capture}}$ which is the effect of K-capture dealignment on the measurement of λ. Thus we could say that $\lambda_{\text{measured}} = \lambda_{\text{true}} + \Delta\lambda_{\text{K-capture}} + \Delta\lambda_{\text{Ionic}}$.

Does an A^i of this size seem reasonable? We can list below considerations of this question.

1. The decay scheme of Co^{58} seems to imply that the 2+ excited level of Fe^{58} (our intermediate state) is a vibrational level. We then expect that the nuclear g-factor (g_N) is about 0.4 instead of 2 as it is before the K-capture. This will introduce a factor tending to make A^i about 1/5 of A.
2. On the other hand, after the Auger cascade has taken place, the ion is optically excited. There may be unpaired 3s or 4s electrons, as well as 3p or 3d electrons. Because of a smaller centrifugal barrier the 3p and 3s electrons will have a much higher probability of being near the nucleus and consequently the coupling associated with these electrons will be much higher than with the 3d.
3. At the same time, the ion will probably be Fe^{+5} (Ref. 35) during the lifetime of the state (2×10^{-11} seconds). This high net charge will pull all electrons in toward the nucleus, and further enhance the hyperfine interaction.

The net effect of considerations 2 and 3 is probably more than a factor of 5, although there is very little evidence. The observed $A^i/A = \frac{0.08}{0.04} = 2$ is not unlikely. A careful study of the expected electronic wave functions in Fe^{+5} would give a more quantitative feeling for the above

considerations. However, more important, it would seem that there is a need for experiments which are explicitly designed to study the K-capture effect.

V.3 THE TRUE NUCLEAR λ

These experiments have almost eliminated the effect of ionic interactions by observing nuclear alignment in a crystal where ionic interactions have nearly vanished. However, the experiments have succeeded in pointing out an effect which has not yet been eliminated and which must be taken into account in evaluating all nuclear alignment experiments.

Because of this K-capture effect, it is impossible to assign a value of the real nuclear λ on the basis of these experiments. No valid independent conformation of the very precise conclusions of Boehm and Wapstra ($\lambda < 0.012$) is yet possible, although such a value is certainly consistent with these experiments. However, the outlook for the future is not completely hopeless. In the 14% of the transitions which go by β-decay we expect no Auger effect, however there may be some optical excitation due to recoil and the sudden change of the nuclear charge (Z). None the less we would expect a smaller coupling (A^i) in the intermediate state. The dealignment goes as $(A^i)^2$. Dealignment following K-capture is observed to be quite small--probably influencing λ by about -0.04. Dealignment following β-decay should be considerably smaller, and we can anticipate that by looking only at those γ's which follow β-decay we would

have an accurate measure of the nuclear λ. By coincidence methods this is possible, although counting rates will be much lower than in these experiments. Of course it is important that this be done in a 0% Ni crystal so that there are no ionic interactions to complicate the problem.

V.4 THE PROPOSAL OF ADDITIONAL EXPERIMENTS

There are numerous experiments which can supply information on nuclear realignment in addition to the one just mentioned. One is to align an isotope which has a completely known decay scheme and which K-captures. In the same 0% Ni crystal a different isotope of the element is aligned. If this second isotope β-decays or has a short lifetime, we can expect that it will be less affected by dealignment and we should be able to predict the $W(\theta)$ of the first isotope by measuring $W(\theta)$ of the second. Deviations from this can be attributed to K-capture dealignment in the first isotope.

An isotope which K-captures and which emits two γ-rays in cascade following the K-capture can be aligned. If the $W(\theta)$ of the two γ-rays is predictable, an experiment can look for deviations in the comparative $W(\theta)$'s of the two γ-rays due to K-capture dealignment. An experiment similar to this has been done for Co^{60} which β-decays however and no effect was observed to the 1/2% accuracy of the experiment (Ref. 39).

VI. CONCLUSIONS

Some nuclear property causes the measured λ to be negative when Co^{58} is aligned in $ZnSiF_6 \cdot 6H_2O$. The only possibility would seem to be nuclear dealignment in the short lived intermediate state which follows K-capture. Except in cases involving nuclei with short lived intermediate states ($\tau < 10^{-11}$ sec), the precision of all nuclear alignment experiments must be questioned for this reason. Only by the superposition of a strong ($\sim$1000 gauss) axial magnetic field can this effect be eliminated.

Interactions between a Co^{58} ion and its paramagnetic environment cause the measured λ to vary with the nickel concentration in $(Ni,Zn)SiF_6 \cdot 6H_2O$. These interactions disturb the measurement of λ most seriously in the 4 to 6 percent nickel concentration range. In the case of other paramagnetic salts (such as the Tutton salts, for instance) it is not possible to say at what concentrations interactions will have the most serious effects. Hence, for precision measurements it seems important that the radioactive material be aligned in a salt which is almost free of paramagnetic isotopes.

APPENDIX I

CRYSTALS

a) Crystal growth

The (Co, Ni, Zn)$SiF_6 \cdot 6H_2O$ crystal is grown from a saturated water solution of $NiSiF_6 \cdot 6H_2O$ and $ZnSiF_6 \cdot 6H_2O$ plus a trace of $Co^{58}Cl_2$. The crystal is started by placing a non-radioactive seed of the appropriate concentration into a 20 ml plastic container of the radioactive solution. (The seeds are obtained by allowing a solution of the fluosilicates to partially evaporate in a wax coated watch glass.) The plastic container is placed in a constant temperature bath and partially covered by foil to keep the evaporation rate low.

The crystals grow into hexagonal columns and weigh about 2.5 gms. The crystals are a light green in color when warm, and are blue at $77^{\circ}K$. The crystals used are visually perfect. Their hexagonal (c) axis is along the axis of the columns.

b) Crystal structure

The structure is of the CsCl type. Figure 14 shows the crystal structure of $NiSiF_6 \cdot 6H_2O$. The structure of $ZnSiF_6 \cdot 6H_2O$ is identical except for dimensions. See Table 9. (Ref. 40).

In our actual crystal the structure is the same as that shown, except any site in figure 14b may be occupied by a Ni, Zn, or Co^{58} ion.

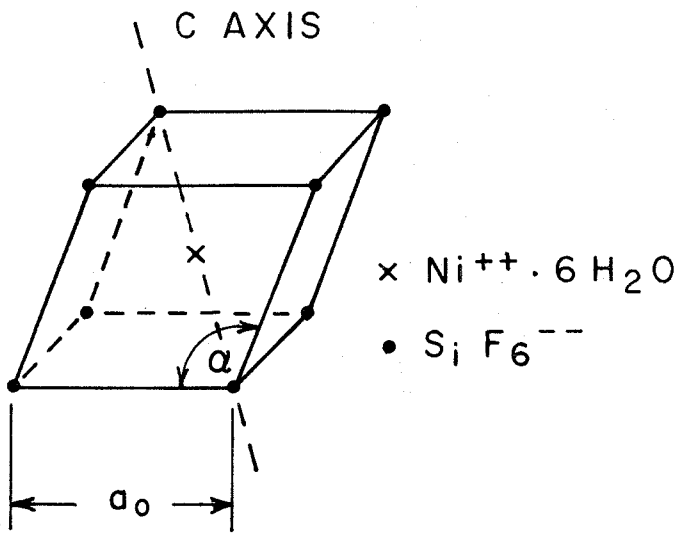

RHOMBOHEDRAL CELL

c axis is the alignment axis

(a)

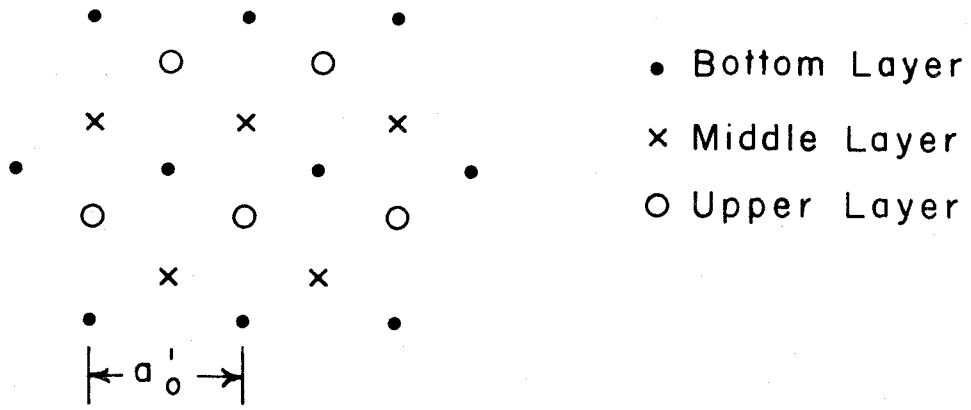

NICKEL SITES

SiF_6^{--} omitted. c axis out of paper.

Distance between layers is $c_o'/3$

(b)

$NiSiF_6 \cdot 6H_2O$ CRYSTAL STRUCTURE

Dimensions are given in Table 9, following page.

FIGURE 14

Table 9

Dimensions of $NiSiF_6 \cdot 6H_2O$
and $ZnSiF_6 \cdot 6H_2O$

	a_o	α	a_o'	c_o'
$NiSiF_6 \cdot 6H_2O$	6.21A	96.3°	9.26A	9.50A
$ZnSiF_6 \cdot 6H_2O$	6.27A	96.1°	9.32A	9.64A

See figure 14 on previous page.

APPENDIX II

THE THERMODYNAMICS OF PARAMAGNETIC SALTS

a) Independent particle case

The entropy per mole of a paramagnetic substance when the ions can be considered as independent is (Ref. 41 and 42):

$$S/Nk = \frac{d\ (T \log Z)}{dt} \qquad (II.1)$$

where the partition function (Z) is:

$$Z = \sum_i e^{-E_i/kT} \qquad (II.2)$$

the sum being taken over all ionic energy levels.

Now, in all our work we can neglect the lattice entropy which is proportional to $(T/T_\theta)^3$ where T_θ is the Debye temperature and is generally 10^2-10^3°K. If the paramagnetic salts have an effective spin (S') equal to $\frac{1}{2}$ and no nuclear spin there are two ionic energy levels. In a magnetic field along one of the susceptibility axes (Section II.2, p. 22):

$$E_+ = +\epsilon = g_\alpha \beta H(\tfrac{1}{2}) \qquad (II.3a)$$

$$E_- = -\epsilon$$

where $\alpha = x$, y, or z.

From equation IV.4 (p.101):

$$E_+/k \text{ (in degrees)} = 3.36 \times 10^{-5}\ g_\alpha H_\alpha \qquad (II.4)$$

where H_α is in gauss. S/Nk vs. kT/ϵ for $S' = \frac{1}{2}$ is plotted in figure 15.

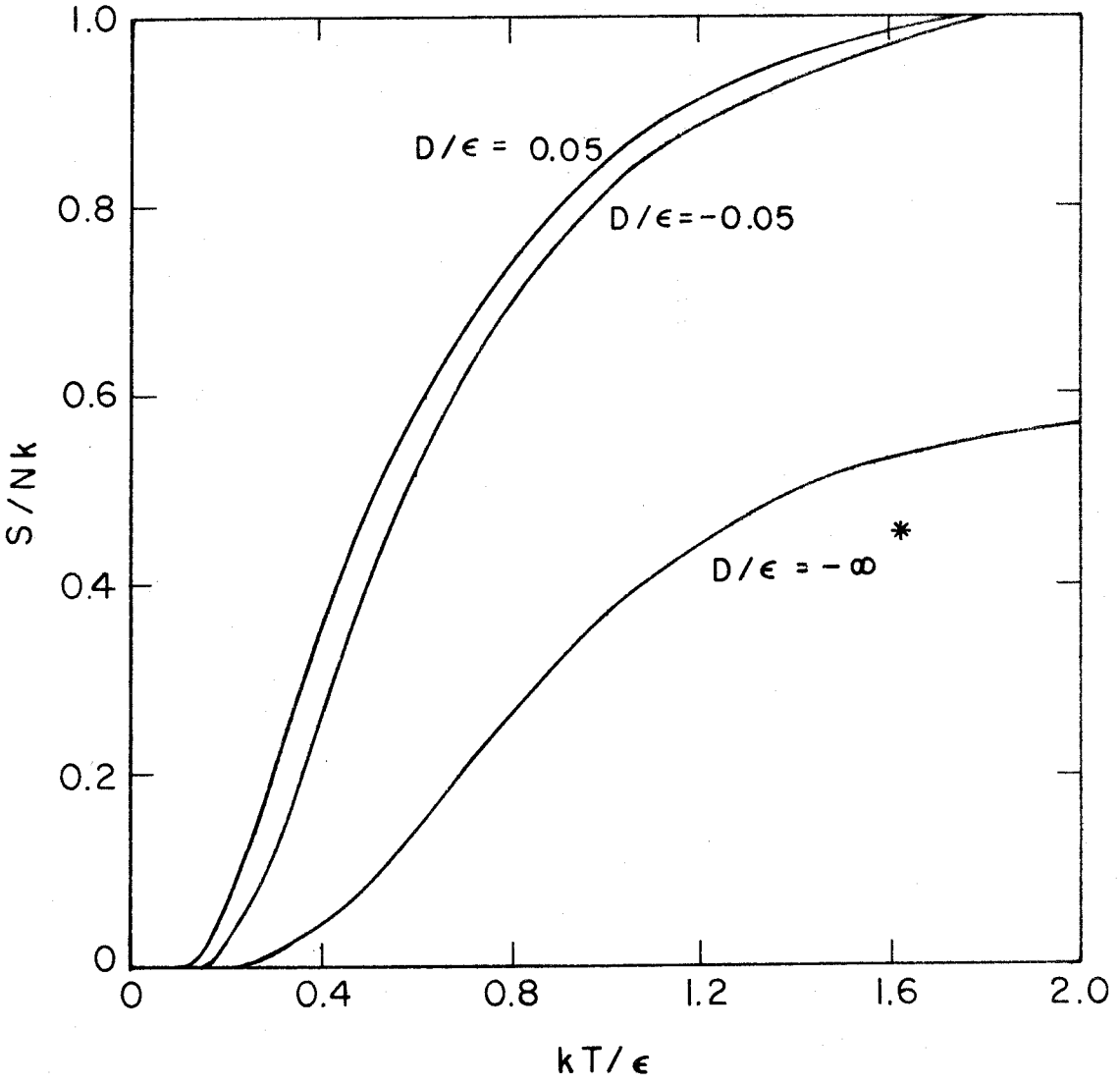

ENTROPY, TEMPERATURE RELATION FOR A

SPIN 1 SYSTEM OF NON-INTERACTING IONS

2ϵ = ground level splitting

N is the number of ions being considered.

* Incidentally, this is also the entropy, temperature relation for a spin 1/2 system.

FIGURE 15

If we are dealing with an ion of effective spin 1 and in a z-directed magnetic field the electronic energy levels are:

$$E_+ = \epsilon + \frac{1}{3} D = g_z \beta H_z (1) + \frac{1}{3} D \qquad \text{(II.5a)}$$

$$E_o = 0 - \frac{2}{3} D \qquad \text{(II.5b)}$$

$$E_- = -\epsilon + \frac{1}{3} D = g_z \beta H_z (-1) + \frac{1}{3} D \qquad \text{(II.5c)}$$

and again from Appendix IV

$$E_+/k \text{ (in degrees)} = 6.72 \times 10^{-5} g_z H_z + \frac{1}{3} D/k \text{ etc.}$$

where H_z is in gauss.

S/Nk vs. kT/ϵ is plotted in figure 15, for three values of D/ϵ. The entropy of $NiSiF_6 \cdot 6H_2O$ in a field of 22,000 gauss and at 0.95^oK can be found by noting that:

$$\epsilon/k = 6.72 \times 10^{-5} \times 2.29 \times 22{,}000 = 3.38^oK$$

$$kT/\epsilon = 0.95/\epsilon = 0.281$$

$$D/\epsilon = -\frac{0.176}{3.38} = -0.05$$

Hence S/Nk = 0.1 after demagnetization.

b) Very low temperature case

Given an initial H and T for a particular salt whose Hamiltonian is known, Section a) enables us to find the entropy per mole of paramagnetic ions. If we knew the entropy

vs. T curve for the system at very low temperatures and in zero field, we could predict how cold the crystal would get after demagnetization merely by equating the initial entropy to the final entropy.

The very low temperature region of this relation for an undiluted salt can be explained using the concept of spin waves. A spin wave is a collective particle excitation quite similar to a phonon. At absolute zero in a ferromagnetic each domain has all its spins parallel. Adding a little energy to the system creates a standing probability wave for finding a spin in the wrong direction. This gives an entropy (S) proportional to $T^{3/2}$ as $T \rightarrow 0$. Kittel (Ref. 43) gives a semiclassical discussion of this subject, while a good quantum treatment is given by Van Kranendonk and Van Vleck (Ref. 44).

At higher temperatures, however, there are so many spin waves that frequent collisions make this concept no longer useful. When the temperature is high compared to the couplings, another approximation is possible which shows $[S/Nk - \log(2S' + 1)] = -(kT)^{-2}$. (Ref. 45).

In a dilute salt after demagnetization the temperatures are too low for this approximation to be valid and we must rely on experimental values. Figure 16 shows some experimental data on $(Zn,Ni)SiF_6 \cdot 6H_2O$ of about 15% Ni. Note the two specific heat peaks--one due to interactions and one due to the "D" term.

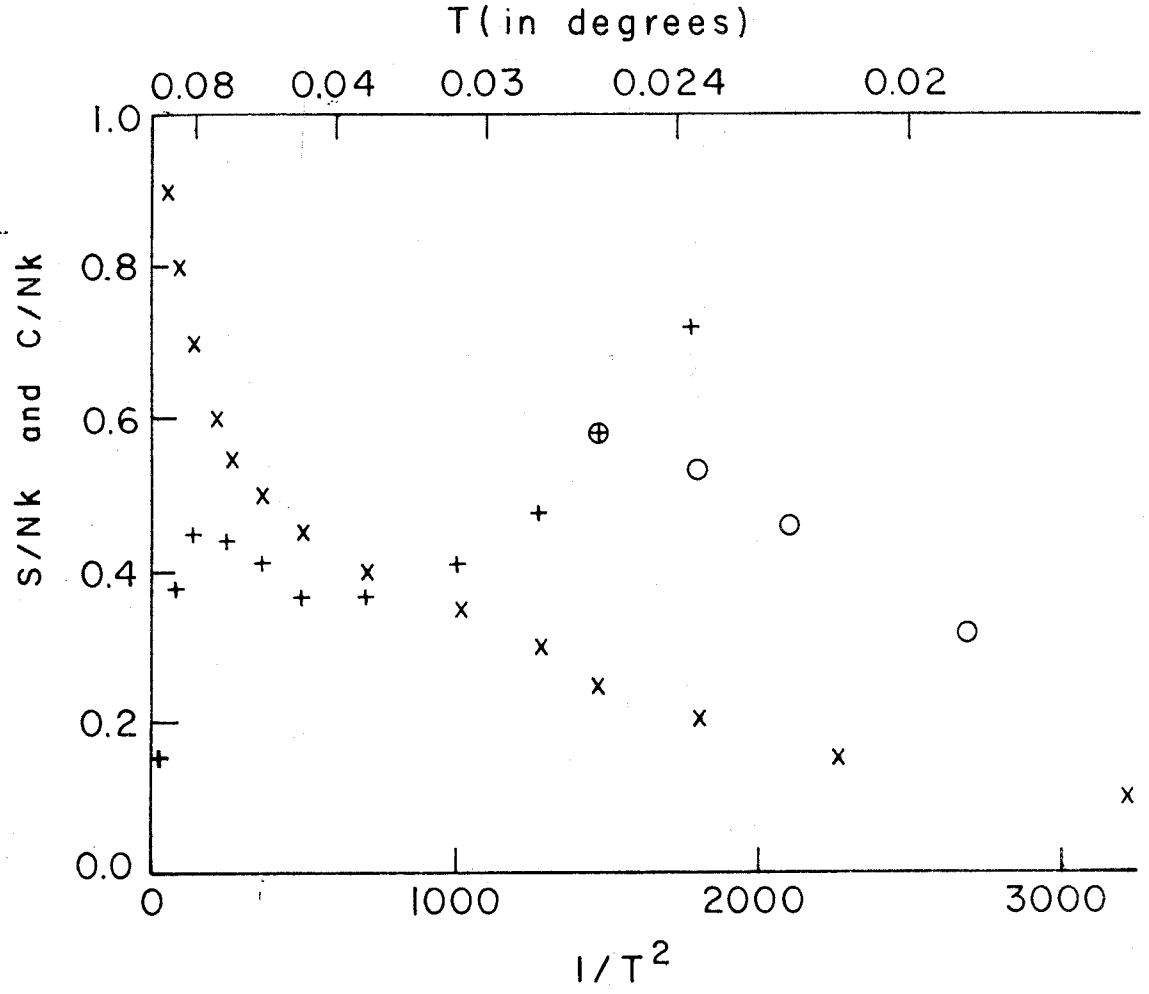

EXPERIMENTAL ENTROPY (S) AND SPECIFIC HEAT (C)

OF $(0.85\ Zn, 0.15\ Ni)SiF_6 \cdot 6H_2O$

N is the number of ions being considered

\+ C/Nk given by Kurti (Ref. 29)

x S/Nk given by Kurti (Ref. 29)

o C/Nk calculated from $C = -2(T^{-2})\frac{dS}{d(T^{-2})}$ and Kurti's entropy values

FIGURE 16

Thus, we would expect to reach a temperature of $0.017^{\circ}K$ ($\frac{1}{T^2} = 3250$) ($\beta = 1.14$) after demagnetization from 22,000 gauss and $0.95^{\circ}K$ ($S/Nk = 0.1$).

This value is actually observed (Table 6, p. 61).

APPENDIX III

THE DECAY OF Co^{58} AND ITS EXPECTED ANGULAR DISTRIBUTION

The decay scheme of Co^{58} is shown in figure 1, p. 4. We shall derive $W(\Theta)$ for the 0.810 Mev γ which follows the 0.470 Mev β-transition. The spin change in the $\beta+$ transition is 0. The β and neutrino can carry off 1 or 0 units of angular momentum and still have a high probability allowed transition. We define λ as the fraction which carry off 0 units of angular momentum (called Fermi decay). $(1-\lambda)$ is the fraction which carry off 1 unit of angular momentum (called Gamow-Teller decay). No other possibilities seem important.*

Consider the fraction, λ , which have L = 0. Equation 13a says:

$$N_k^i f_k^i = N_k^o f_k^o \qquad \text{(III.1)}$$

---

*1. One possibility is that the ground state of Co^{58} is 1+ not 2+. However, this assumption would give $W(\Theta)$'s which are unambiguously inconsistent with this experiment.

2. Another possibility is the ground state of Co^{58} is 2-. This would make the 0.470 Mev transition first-forbidden instead of allowed. However, log ft is found to be 6.6 in line with an allowed transition instead of the 8 to 9 expected from a first-forbidden transition.

3. An admixture of second-forbidden decay could be important, however log ft should be 11.6 to 13.4 compared to 6.6 observed for the decay. Thus the admixture should be down by a factor of $\sim 10^{-5}$. It would take an admixture of 10^{-2} to influence this experiment.

now, since the γ decay is quadrupole, and $I_f = I_i - 2$ we use equation 10a which becomes:

$$W_o(\theta) = 1 - \frac{15}{7} N_2^o f_2^o P_2(\cos\theta) - 5 N_4^o f_4^o P_4(\cos\theta) \qquad \text{(III.2)}$$

We now have $W(\theta)$ in terms of f_k^o's instead of f_k^i's. $W(\theta)$ for $L = 0$ is now, using equation 12a for the N's:

$$W_o(\theta) = 1 - \frac{10}{7} f_2^o P_2(\cos\theta) - \frac{40}{3} f_4^o P_4(\cos\theta) \qquad \text{(III.3)}$$

For the fraction, $(1-\lambda)$, with $L = 1$ we get, similarly using equation 13c in equation 10a

$$W_1(\theta) = 1 - \frac{5}{7} f_2^o P_2(\cos\theta) + \frac{80}{9} f_4^o P_4(\cos\theta) \qquad \text{(III.4)}$$

Taking

$$W(\theta) = \lambda W_o(\theta) + (1-\lambda) W_1(\theta) \qquad \text{(III.5)}$$

We have

$$W(\theta) = 1 - \frac{5}{7}(1+\lambda) f_2^o P_2(\cos\theta) + \frac{40}{9}(2-5\lambda) f_4^o P_4(\cos\theta) \qquad \text{(III.6)}$$

APPENDIX IV

NUMERICAL CONVERSION OF THE Co^{59} SPIN HAMILTONIAN TO TEMPERATURE UNITS AND TO Co^{58}

a) Units

In spectroscopic notation an energy of 0.0184 cm^{-1} is the energy of a photon of wavelength (λ) = 1/0.0184. This energy (E) is

$$E = h\nu = hc/\lambda = (hc)(0.0184) \qquad (IV.1)$$

We want to use "temperature units" i.e., an energy of 1° is 1k. Thus to convert 0.0184 cm^{-1} to temperature units we find

$$E/k \text{ (in degrees)} = \frac{hc}{k}(0.0184)$$

$$= 1.438\ (0.0184)$$

$$= 0.0264 \qquad (IV.2)$$

similarly, 0.0047 cm^{-1} becomes:

$$E/k \text{ (in degrees)} = (1.438)(0.0047) = 0.00675 \qquad (IV.3)$$

Examine the $g_{\parallel} \beta H_z S_z$ term in equation 16. If we put in the value of β (0.927×10^{-20} ergs/gauss) and divide by k (1.38×10^{-16} ergs/$^{\circ}$K) we have

$$g_{\parallel} \beta H_z S_z \text{ (in degrees)} = 6.72 \times 10^{-5}\ g_{\parallel} H_z S_z \qquad (IV.4)$$

where

H_z is in gauss.

Putting in values of $g_{\parallel}$ and $g_{\perp}$ into equation IV.4 and using equations IV.2 and IV.3 in equation 16 we have for Co^{59} in $ZnSiFi \cdot 6H_2O$:

$$\mathcal{H}/k = 3.91 \times 10^{-4} H_z S_z + 2.31 \times 10^{-4} (H_x S_x + H_y S_y)$$

$$+ 0.0264 S_z I_z + 0.00675 (S_x I_x + S_y I_y) \qquad \text{(IV.5)}$$

b) Co^{59} to Co^{58} Conversion

The hyperfine terms in equation IV.5 must be adjusted to allow for the fact that the magnetic moment, and the spin of Co^{58} is different from that of Co^{59}. Now "A" is a measure of the effective field (H_{eff}) of the electrons at the nucleus times the magnetic moment of the nucleus. The total energy (ΔE) from changing I_z from +I to -I is

$$\Delta E = A S_z 2I = 2 H_{eff} \mu_N \qquad \text{(IV.6)}$$

where

μ_N is the magnetic moment of a particular isotope.

For a different isotope, however,

$$\Delta E' = A' S_z 2I' = 2 H_{eff} \mu_N' \qquad \text{(IV.7)}$$

assuming H_{eff} is independent of the isotope.

Dividing equation IV.6 by equation IV.7 we have

$$AI/A'I' = \mu_N/\mu_N' \qquad \text{(IV.8)}$$

Now from (Ref. 46):

$I = 7/2$ for Co^{59}

$I = 2$ for Co^{58}

and

$$\mu_{58}/\mu_{59} = 0.8734 \pm 0.0024$$

Using equation IV.8, equation IV.5 becomes:

$$\mathcal{H}/k = 3.91 \times 10^{-4} H_z S_z + 2.31 \times 10^{-4} (H_x S_x + H_y S_y) + 0.0403 S_z I_z + 0.0103 (S_x I_x + S_y I_y) \qquad \text{(IV.5)}$$

for Co^{58}.

The above reference allows us to treat Co^{60} in an identical manner.

$$\mathcal{H}/k = 3.91 \times 10^{-4} H_z S_z + 2.31 \times 10^{-4} (H_x S_x + H_y S_y) + 0.0152 S_z I_z + 0.0039 (S_x I_x + S_y I_y) \qquad \text{(IV.6)}$$

for Co^{60}.

APPENDIX V

CALCULATION OF NUCLEAR POPULATIONS WHEN $|S_z, I_z\rangle$ IS NOT AN EIGENFUNCTION OF THE HAMILTONIAN

If we are dealing with a mixed state, where $|S_z, I_z\rangle$ is not diagonal in the Hamiltonian, we calculate the expectation value of the k'th moment of the nuclear spin $[\langle (I_z)^k \rangle_\mu]$ for a particular state (ψ_μ) as:

$$\langle (I_z)^k \rangle_\mu = \langle \psi_\mu | (I_z)^k | \psi_\mu \rangle \tag{V.1}$$

if

$$\psi_\mu = b_{\mu S_z I_z} | S_z, I_z \rangle + b_{\mu S_z' I_z'} | S_z', I_z' \rangle \tag{V.2}$$

using the properties of $\langle \ | \ | \ \rangle$ we have

$$\begin{aligned} \langle (I_z)^k \rangle_\mu = {} & b^*_{\mu S_z I_z} b_{\mu S_z I_z} \langle S_z, I_z | (I_z)^k | S_z, I_z \rangle \\ & + b^*_{\mu S_z I_z} b_{\mu S_z' I_z'} \langle S_z, I_z | (I_z)^k | S_z', I_z' \rangle \\ & + b^*_{\mu S_z' I_z'} b_{\mu S_z I_z} \langle S_z', I_z' | (I_z)^k | S_z, I_z \rangle \\ & + b^*_{\mu S_z' I_z'} b_{\mu S_z' I_z'} \langle S_z', I_z' | (I_z)^k | S_z', I_z' \rangle \end{aligned} \tag{V.3}$$

But since

$$\left\langle S'_z, I'_z \left| (I_z)^k \right| S_z, I_z \right\rangle = (I'_z)^k \, \delta_{I_z I'_z} \, \delta_{S_z S'_z} \qquad (V.4)$$

$$\left\langle (I_z)^k \right\rangle_\mu = (I_z)^k \left| b_{\mu S_z I_z} \right|^2 + (I'_z)^k \left| b_{\mu S'_z I'_z} \right|^2 \qquad (V.5)$$

generalizing when many states are mixed

$$\left\langle (I_z)^k \right\rangle_\mu = \sum_{S'_z I'_z} (I'_z)^k \left| b_{\mu S'_z I'_z} \right|^2$$

APPENDIX VI

THE EFFECT OF THE WEAK Co^{58} γ-RAYS ON THE MEASURED λ.

Figure 1 (p. 4) gives the decay scheme of Co^{58}. The weak 0.81 Mev γ-ray from the 1.62 Mev level, and the 0.81 Mev γ-ray which follows both are counted and contribute to the observed angular distribution of the 0.81 Mev γ-ray following the 0.47 Mev beta-decay.

The angular distribution of the first γ-ray in the cascade is (Ref. 26):

$$W_1(\theta) = 1 + \frac{(-0.5 + 1.46\delta + 0.154\delta^2)(1 + \lambda')}{(\delta^2 + 1)} f_2 P_2(\cos\theta) + \frac{1.27\delta^2}{\delta^2 + 1}(-2 + 5\lambda') f_4 P_4(\cos\theta) \qquad \text{(VI.1)}$$

The angular distribution of the second γ-ray in the cascade is:

$$W_2(\theta) = 1 - \frac{5}{7}(1 + \lambda') \frac{(1/2 - 3/4\,\delta^2)}{(1 + \delta^2)} f_2 P_2(\cos\theta) + \frac{40}{9}(2 - 5\lambda') \frac{(2/3 - 1/14\,\delta^2)}{(1 + \delta^2)} f_4 P_4(\cos\theta) \qquad \text{(VI.2)}$$

where

λ' is the λ associated with the electron capture to the 1.62 Mev level

f_k are the alignment parameters for the initial Co^{58} state

$\delta = \frac{a_2}{a_1}$ = intensity ratio of quadrupole and dipole components of radiation.

Now, we know that $\lambda' = 0.2$ (Ref. 28) and that $\delta = -2.2$ (Ref. 18).* When we compare the above angular distributions with the distribution of the principal γ-ray:

$$W(\theta) = 1 - \frac{5}{7}(1 + \lambda) f_2 P_2(\cos\theta) + \frac{40}{9}(2 - \lambda) f_2 P_4(\cos\theta) \qquad \text{(III.6)}$$

We see that only the P_2 term in equation VIII.1 is important. This term is about 0.8 that of the corresponding term for the principal γ-ray.

Now, the observed distribution $W_o(\theta)$ is

$$W_o(\theta) = \frac{0.984 W(\theta) + 0.016 W_1(\theta) + 0.016 W_2(\theta)}{1.016} \qquad \text{(VI.5)}$$

Consider the effect if $\beta = 1.5$ the coefficient of P_2 for the principal γ-ray is 0.199. Then we have:

$$W_1(0^\circ) \approx 1 - (0.8)(0.199) = 0.84 \qquad \text{(VI.6a)}$$

$$W_1(90^\circ) \approx 1 + (0.8)(0.5)(0.199) = 1.08 \qquad \text{(VI.6b)}$$

$$W_2(0^\circ) \approx W_2(90^\circ) \approx 1 \qquad \text{(VI.6c)}$$

---

*Fraunfelder et al (Ref. 18) state that $\delta = +2.2$ from angular correlation studies. However, the theoretical relations used by Fraunfelder have a different sign convention for δ (Ref. 47).

$$W(0^{\circ}) = 0.8416 \qquad \text{for} \quad \lambda = 0 \qquad \text{(VI.6d)}$$

$$W(90^{\circ}) = 1.1150 \qquad \text{for} \quad \lambda = 0 \qquad \text{(VI.6e)}$$

Hence, using equation VI.5

$$W_o(\theta) = 0.8440$$

$$W_o(\theta) = 1.1126$$

This point has a measured λ of -0.003. If $\beta = 1.0$ or ∞ is the measured λ is still about -0.003. A correction of +0.003 has been made to all the measured λ's given in this report.

APPENDIX VII

CORRECTIONS

There is a certain number of background counts (principally from cosmic rays) which must be subtracted from the warm counts and the cold counts before $W(\theta)$ is calculated. Table 10 gives the fraction of the total warm counts which were noise in the various crystals.

Since there is about 0.03 μcuries of Co^{60} for each μcurie of Co^{58} in the Oak Ridge source, some of the observed counts are due to Co^{60}, and a correction is needed. This correction is made by experimentally determining the fraction of warm counts which are Co^{60}, then subtracting that fraction from the warm counts. From the cold counts we subtract the same fraction, adjusted for the expected theoretical $W(\theta)$ for Co^{60} at that angle. Table 10 gives the percentage of Co^{60} in the Co^{58} and Table 11 gives the correction to be added to $W(\theta)$ at various "temperatures". [For purposes of these corrections a temperature is defined by $W(0^{\circ})$.]

Figure 17 gives the angular distribution for the principal 810 kev γ-ray for two values of β with $\lambda = 0$. By averaging $W(\theta)$ over the solid angle of the counter a correction to be added to the observed $W(\theta)$ is obtained.

For the 6%, 12%, 19%, and first night's runs of the first 0% crystal the half angle subtended by the 0 counter

Table 10

Noise and Co^{60} in Co^{58}

Crystal	Percent Noise 0^{o}	Percent Noise 90^{o}	Percent Co^{60} Counts in Co^{58} Counts 0^{o}	Percent Co^{60} Counts in Co^{58} Counts 90^{o}
6%	2.4	0.67	1.1	1.0
12%	2.7	6	1.7	1.8
19%	1.9	0.5	1.0	1.0
1st 0%	3*	1*	0.8	1.4
2nd 0%	7	2.5	0.8	1.4
4%	15	7.2	0.9	0.9

*First night's runs

Table 11

Co^{60} and Solid Angle Corrections

	Co^{60} correction*		Solid angle correction**	
W(0)	$\Delta W(0^\circ)$	$\Delta W(90^\circ)$	$\Delta W(0^\circ)$	$\Delta W(90^\circ)$
0.82	+.002	0.000	0.000	+0.007
0.84	+.002	0.000	-0.001	+0.004
0.88	+.002	0.000	-0.001	+0.002
0.92	+.001	0.000	0.000	+0.001

*Co^{60} correction is for 1% Co^{60} in Co^{58}

**Solid angle correction is for 7° and 10° half angles. It must be doubled for 9.6° and 13.8° half angles.

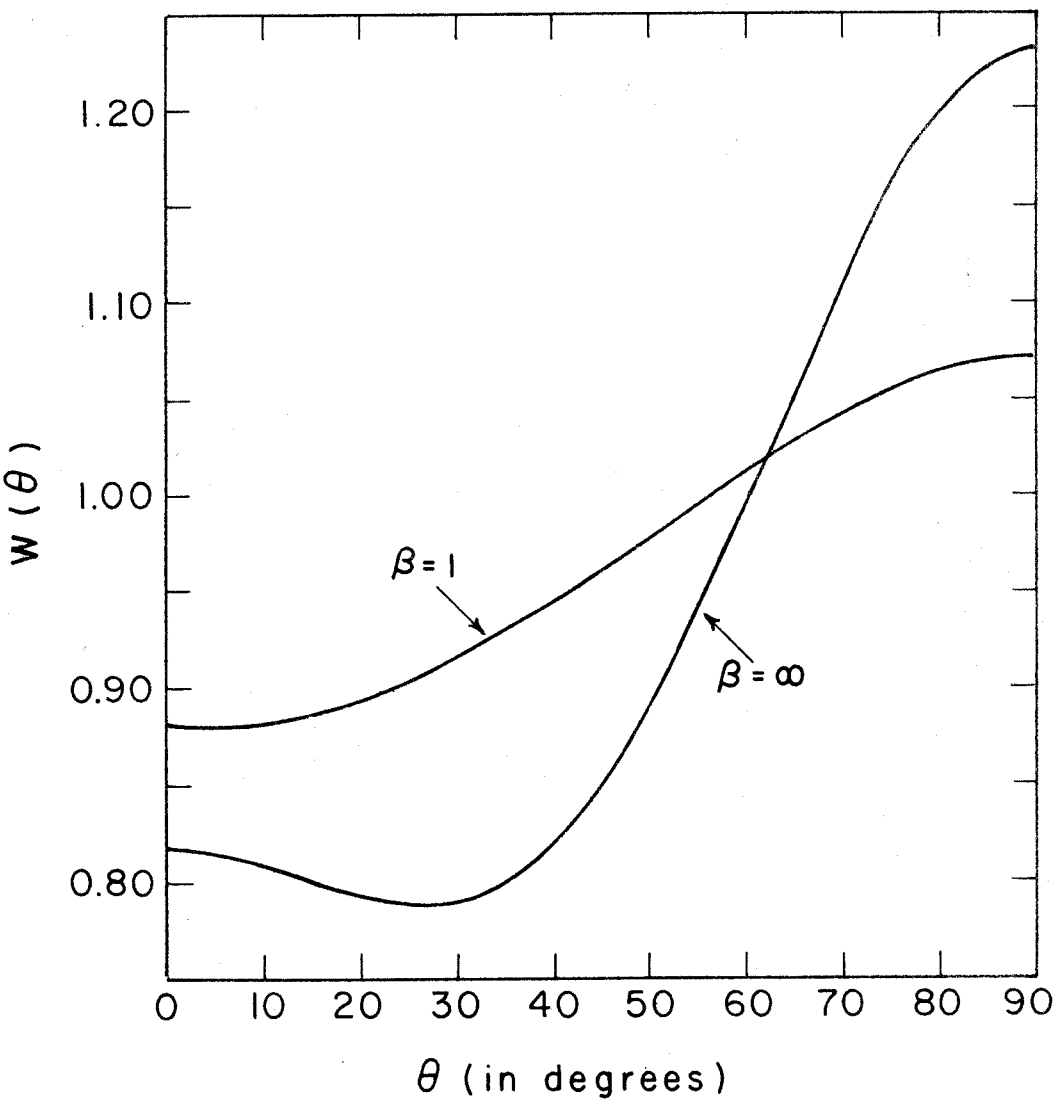

THEORETICAL NORMALIZED COUNTING RATE W(θ)

VERSUS θ FOR Co^{58}

Curves are for the case of $\lambda = 0$.

We have used the theory for the ideal case of Co^{58} in $ZnSiF_6 \cdot 6H_2O$ (Section II).

FIGURE 17

was 7° and the half angle of the 90° counter was 10°. For the second night's runs of the first 0% crystal, the second 0%, and the 4% crystal the half angles were 9.6° and 13.8° respectively.

APPENDIX VIII

CHECK FOR STATISTICAL SIGNIFICANCE OF DATA

The series of demagnetizations (runs) made on each crystal yields a series of measured λ's (each λ is now averaged over all temperatures) and associated statistical counting errors (σ_s). In addition there is an error associated with shifts in the electronics and any other non-counting fluctuations. We assume these unknown fluctuations can be assigned a quantity (σ_e) which takes them into account and is constant for all (n) runs, made on a given evening. Any run (i) then has a total error:

$$\sigma_i^2 = \sigma_{s,i}^2 + \sigma_e^2 \qquad \text{(VIII.1)}$$

We now define a quantity (ϵ) (Ref. 48):

$$\sum_i^n \frac{(\Delta\lambda_i / \sigma_i)^2}{n-1} = \epsilon \qquad \text{(VIII.2)}$$

where

$$\Delta\lambda_i = \lambda_i - \bar{\lambda} \qquad \text{(VIII.3)}$$

and λ_i is the value of λ for run i averaged over all the counts in that run and where

$$\bar{\lambda} = \frac{\sum_i \lambda_i / \sigma_i^2}{\sum_i 1/\sigma_i^2} \qquad \text{(VIII.4)}$$

σ_i is the total error (σ) for run i.

If we have picked a correct value for σ_e, then we expect.*

$$\epsilon \approx 1 \qquad \text{(VIII.5)}$$

Table 12 gives values for λ_i, and σ_s for the 0%, 6%, 12%, and 19% crystals. Estimates of σ_e are given, as well as the resulting λ's and ϵ's for each night.

---

*Because the number of runs is small, we expect that equation VIII.5 is only approximately true.

Table 12

Test of Statistical Significance of the Data

Run #	λ_i	Statistical Counting Error $(\sigma_{s,i})$	Electronics and Other Errors (σ_e)	* $\left(\frac{\lambda_i - \bar{\lambda}}{\sigma_i}\right)^2$
		6%, First Night		
4	0.069	0.267	0.028	0.307
5	-0.1538	0.037	0.028	2.585
6	-0.0755	0.0161	0.028	0.015
7	0.001	0.0455	0.028	2.285
	$\bar{\lambda} = -0.080 \pm 0.025$	$\epsilon = 1.5$**		
		6%, Second Night		
1	-0.099	0.041	0.014	0.558
2	-0.140	0.021	0.014	0.167
3	-0.133	0.015	0.014	0.012
	$\bar{\lambda} = -0.131 \pm 0.015$	$\epsilon = 0.4$		
		6%, Third Night		
7	-0.125	0.060	0.016	0.303
8	-0.105	0.015	0.016	0.403
9	-0.097	0.022	0.016	0.052
10	-0.048	0.026	0.016	1.957
	$\bar{\lambda} = -0.091 \pm 0.015$	$\epsilon = 0.9$		
		12%		
1	-0.055	0.0145	0.032	0.129
2	-0.033	0.0110	0.032	0.081
3	-0.078	0.0132	0.032	1.073
4	-0.005	0.0132	0.032	1.182
	$\bar{\lambda} = -0.042 \pm 0.017$	$\epsilon = 0.8$		

Table 12 (continued)

Run #	λ_i	$(\sigma_{s,i})$	(σ_e)	$\left(\frac{\lambda_i - \bar{\lambda}}{\sigma_i}\right)^2$
		19%		
1	0.083	0.038	0.032	2.004
2	0.024	0.028	0.032	0.068
3	-0.003	0.025	0.032	0.157
4	-0.024	0.022	0.032	0.923
	$\bar{\lambda} = +0.024 \pm 0.021$		$\epsilon = 1.0$	
	0%, First crystal, First Night			
2	-0.072	0.020	0.019	0.684
3	-0.038	0.0144	0.019	0.202
4	-0.011	0.0172	0.019	2.12
5	-0.055	0.0190	0.019	0.05
6	-0.094	0.0292	0.019	1.65
	$\bar{\lambda} = -0.049 \pm 0.012$		$\epsilon = 1.2$	
	0%, First crystal, Second Night			
6A	-0.140	0.054	0.049***	2.30
8	+0.014	0.013	0.035	1.39
9	-0.035	0.015	0.035	0.02
10	-0.040	0.015	0.035	0.08
	$\bar{\lambda} = -.030 \pm 0.021$		$\epsilon = 1.3$	
	0%, Second crystal, First Night			
1	0.019	0.0169	0.018	4.775
2	-0.047	0.0084	0.018	0.381
3	-0.040	0.0078	0.018	0.071
4	-0.040	0.0126	0.018	0.056
5	-0.050	0.0118	0.018	0.501
	$\bar{\lambda} = -0.035 \pm 0.10$		$\epsilon = 1.4$	

Table 12 (continued)

Run #	λ_i	$(\sigma_{s,i})$	(λ_e)	$\left(\frac{\lambda_i - \bar{\lambda}}{\sigma_i}\right)^2$
	0%, Second crystal, Second Night			
1	-0.055	0.0087	0.014	0.067
2	-0.032	0.0084	0.014	1.294
3	-0.077	0.0088	0.014	2.497
4	-0.040	0.0101	0.014	0.378
5	-0.049	0.0090	0.014	0.001

$\bar{\lambda} = -0.051 \pm 0.0075 \quad \epsilon = 1.1$

* $\sigma_i^2 = \sigma_{s,i}^2 + \sigma_e^2$

** $\epsilon = \sum_1^n \left(\frac{\lambda_i - \bar{\lambda}}{\sigma_i}\right)^2 \Big/ n-1$

*** There is reason to expect that there was a larger shift in this run.

APPENDIX IX

THE HIGH TEMPERATURE LIMIT

The method of Daniels (Ref. 31) uses the density matrix (ρ) of quantum statistical mechanics to obtain the effect of the $P(\vec{S}_i,\vec{S}_j)$ terms on f_2 and f_4. Tolman (Ref. 49) explains the density matrix clearly, and Daniels' treatment of the problem is quite complete.

This attack yields Δf_2 and Δf_4 as a power series in $P(\vec{S}_i,\vec{S}_j)/kT$ and $D(\vec{S}_i)/kT$ (see equation 30, p. 54, for the meaning of these terms). Here Δf_2 and Δf_4 are the change in f_2 and f_4 due to including these P and D terms in the Hamiltonian.

The first non-vanishing term in Daniels' general calculation is the order of

$$A^2 P_{oj}^{\ 2}/(kT)^4 \qquad \text{(IX.1)}$$

where

P_{oj} is a particular $P(\vec{S}_o,\vec{S}_j)$ which describes the energy of interaction of the cobalt ion of interest (ion o) and another paramagnetic ion, j

A is the coefficient of $S_{o,z}I_{o,z}$ in $\mathcal{H}$ (Eq. 30).

However, in the treatment of a Co^{++} ion surrounded by occasional Ni^{++} ions this term vanishes because of symmetry,

and higher order terms are quite difficult to calculate. As a matter of fact, this whole approach fails for temperatures less than 0.15°. The reason is that the higher order terms look like $A^2 P_{oj}^2 D_j^n/(kT)^{4+n}$ where D_j from equation 33 is $0.176^{\circ}K$. In the temperature range of interest ($0.02^{\circ}KO$ $D/kT = 10$ and the series expansion will fail to converge.

This method will be useful, however, in the case of a paramagnetic crystal where the majority of the paramagnetic ions have $S = 1/2$. In this case, there is no D term (Section IV.1b), and the series will converge quickly for $kT > PA$.

APPENDIX X

EXCHANGE IN $CoSiF_6 \cdot 6H_2O$ AND IN $NiSiF_6 \cdot 6H_2O$

A sample of $CoSiF_6 \cdot 6H_2O$ has been put (Ref. 50) into a magnetic field strong enough to completely align it. The interaction energy (E_i) of an ion with its magnetized environment was found to be:

$$E_i/k = 2.25^{\circ}K \tag{X.1}$$

In addition, specific heat measurements have shown that the magnetic Curie point (θ) for $NiSiF_6 \cdot 6H_2O$ is $0.1^{\circ}K$ (Ref. 51). Kittel (Ref. 43) Chapter 15 shows that:

$$E_i/k = \frac{3\theta S}{S+1} \tag{X.2}$$

Hence, for Ni-Ni exchanges ($S = 1$)

$$E_i/k = 0.15^{\circ}K \tag{X.3}$$

or

$$E_i\big|_{Co} = 7\, E_i\big|_{Ni} \tag{X.4}$$

It should be noted that in the previous discussion no distinction was made between an isotropic exchange ($\vec{S}_i \cdot \vec{S}_j$) between two ions i and j and an anisotropic exchange having a magnetic dipole form of coupling. In $CoSiF_6 \cdot 6H_2O$ there is

no evidence of how much of each type there is. In $NiSiF_6 \cdot 6H_2O$ the speculation is that they are about equal (Ref. 51).

APPENDIX XI

INVESTIGATION OF THE EFFECTS OF INTERACTION ON DEGREE OF ALIGNMENT

A crystal (Fig. 18) was grown which contained about 0.9 μcuries of Co^{58} in pure $ZnSiF_6 \cdot 6H_2O$. It was surrounded by a non-active $ZnSiF_6 \cdot 6H_2O$ blanket which separated it from a 12% nickel layer containing about 0.3 μcuries of Co^{60}. This crystal was aligned and $W(0^\circ)$ of Co^{60} and $W(0^\circ)$ of Co^{58} were obtained (Fig. 19). Plotted on the same graph is a theoretical curve which assumes the Co^{58} and Co^{60} are at the same temperature, and that there are no interactions, or K capture effects.* Also on the graph are results of a similar experiment done with Co^{58} and Co^{60} evenly distributed in a 12% crystal. All of these results are fully corrected.

It appears that interactions in 12% nickel material do not effect $W(0^\circ)_{58}$ in the low temperature region ($\beta = 1.3$). However, in the higher temperature range ($\beta = 0.9$) $W(0^\circ)_{58}$ without interactions is less than $W(0^\circ)_{58}$ with interactions. Thus, the overall picture is that the presence of interactions tends to decrease the "nuclear alignment" as measured by $W(0^\circ)$. This is consistent with the fact that the 0%

---

*Co^{60} has two intense quadrupole γ-rays following a β-decay (Ref. 36). Both γ's have the same theoretical angular distribution and are simultaneously observed. The theoretical angular distribution for Co^{60} with no interactions is obtained in exactly the same manner as for Co^{58} (Section II).

material cooled indirectly by 12% material showed more alignment than the homogeneous 12% crystal (Figs. 8 and 6, pages 46 and 44).

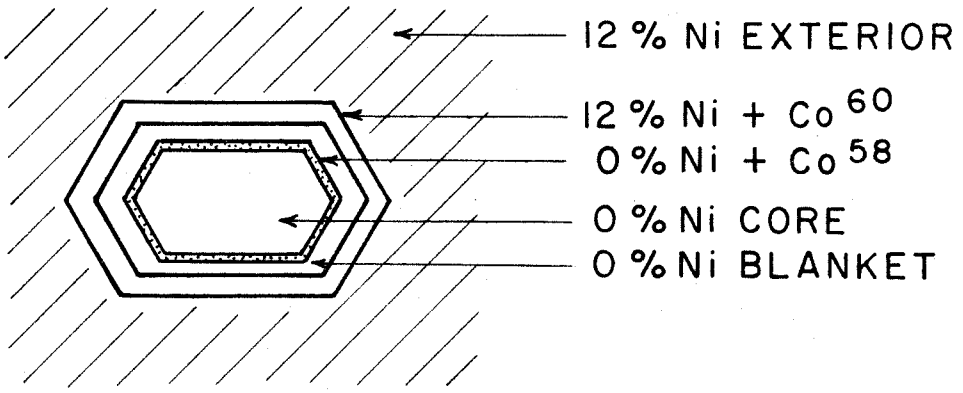

SCALE : 10 : 1

STRUCTURE OF

LAYERED 12% Ni + Co^{60} AND 0% Ni + Co^{58} CRYSTAL

Cross section perpendicular to the axis of alignment

FIGURE 18

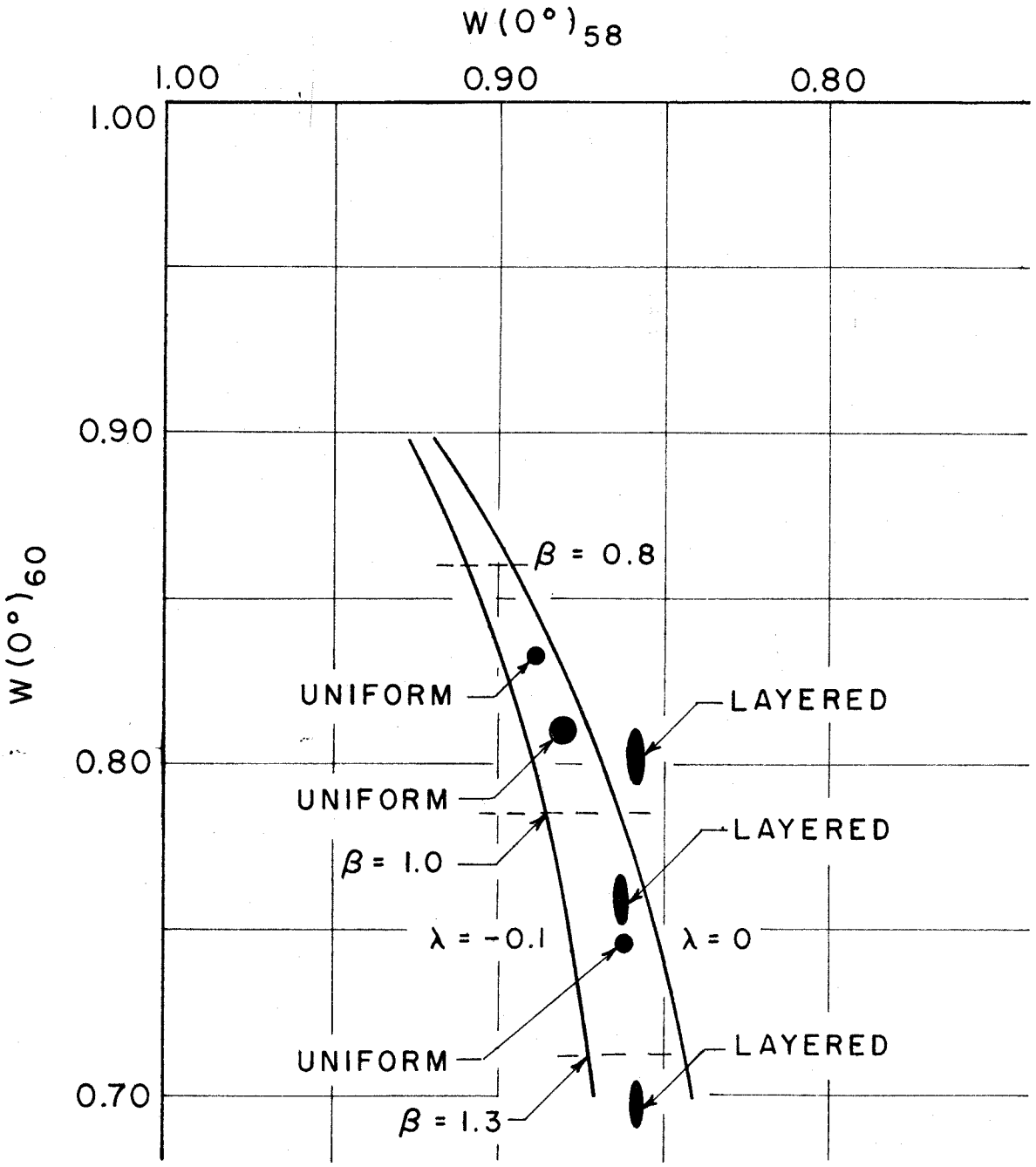

W(0°) FOR Co^{58} VERSUS W(0°) FOR Co^{60} IN A LAYERED 12% Ni + Co^{60} AND 0% Ni + Co^{58} CRYSTAL ALSO FOR A UNIFORM 12% CRYSTAL

Curves are theory with no interactions or K-capture effects. The spin Hamiltonians are those of Appendix IV with $H_{x,y,z} = 0$ They apply to both the 1.17 and 1.33 Mev Co^{60} γ-rays.

FIGURE 19

APPENDIX XII

Co^{58} AND Co^{60} ALIGNED IN $Ce_2Mg_3(NO_3)_{12}\cdot 24H_2O$

a) Introduction

Before doing any experiments with the fluosilicates, experiments were done using traces of Co^{58} in $Ce_2(Mg,Co^{58})_3(NO_3)_{12}\cdot 24H_2O$. A 600 gauss external field was applied along the z-alignment axis (see page 1, idem #2).

This is a poor salt to use for obtaining nuclear information. There are two non-equivalent lattice sites for a cobalt ion. Site I containing about 2/3 of the coablt ions has the spin Hamiltonian for Co^{59} (Ref. 21):

$$\mathcal{H}_I(cm^{-1}) = 4.1\ \beta H_z S_z + 4.4\ \beta (H_x S_x + H_y S_y)$$

$$+ 0.0085\ (S_z I_z) + 0.0103\ (S_x I_x + S_y I_y) \quad \text{(XII.1a)}$$

Site II containing the remaining ions has:

$$\mathcal{H}_{II}(cm^{-1}) = 7.3\ \beta (H_z S_z) + 2.3\ \beta (H_x S_x + H_y S_y)$$

$$+ 0.028\ (S_z I_z) + 0.0000\ (S_x I_x + S_y I_y) \quad \text{(XII.1b)}$$

These results are obtained by paramagnetic resonance using traces of Co^{59} in $\underline{Bi}_2Mg_3(NO_3)_{12}\cdot 24H_2O$. Despite this the constants in the above Hamiltonians are probably correct to 10%. However, the ratio of ionic populations (a_{II}/a_I) in

the two sites is uncertain. This fact, combined with Ce being paramagnetic and contributing an unknown interaction effect make the interpretation of the results very difficult.

b) Results and conclusions

The theoretical curves are obtained merely by converting the Hamiltonians to be applicable to Co^{58} and to Co^{60}, and by putting them into temperature units. The procedure is exactly as in Appendix IV. Then the Hamiltonians are diagonalized as in Section II.3 with $G_{\parallel} \neq 0$ this time. This is done easily by hand since G_x and G_y are still 0.

The values of $W(0^\circ)$ and $W(90^\circ)$ are obtained for each site using the statistical mechanics of Section II.4 at various temperatures and λ's. The observed W's are the weighted average of the W's for each site.

This average is taken for several different population ratios (a_{II}/a_I) and is plotted in figure 20 along with experimental results for a 4 gm crystal. If the real population ratio is near to 0.3/0.7 the results are similar to those obtained in the fluosilicates (Appendix XI).

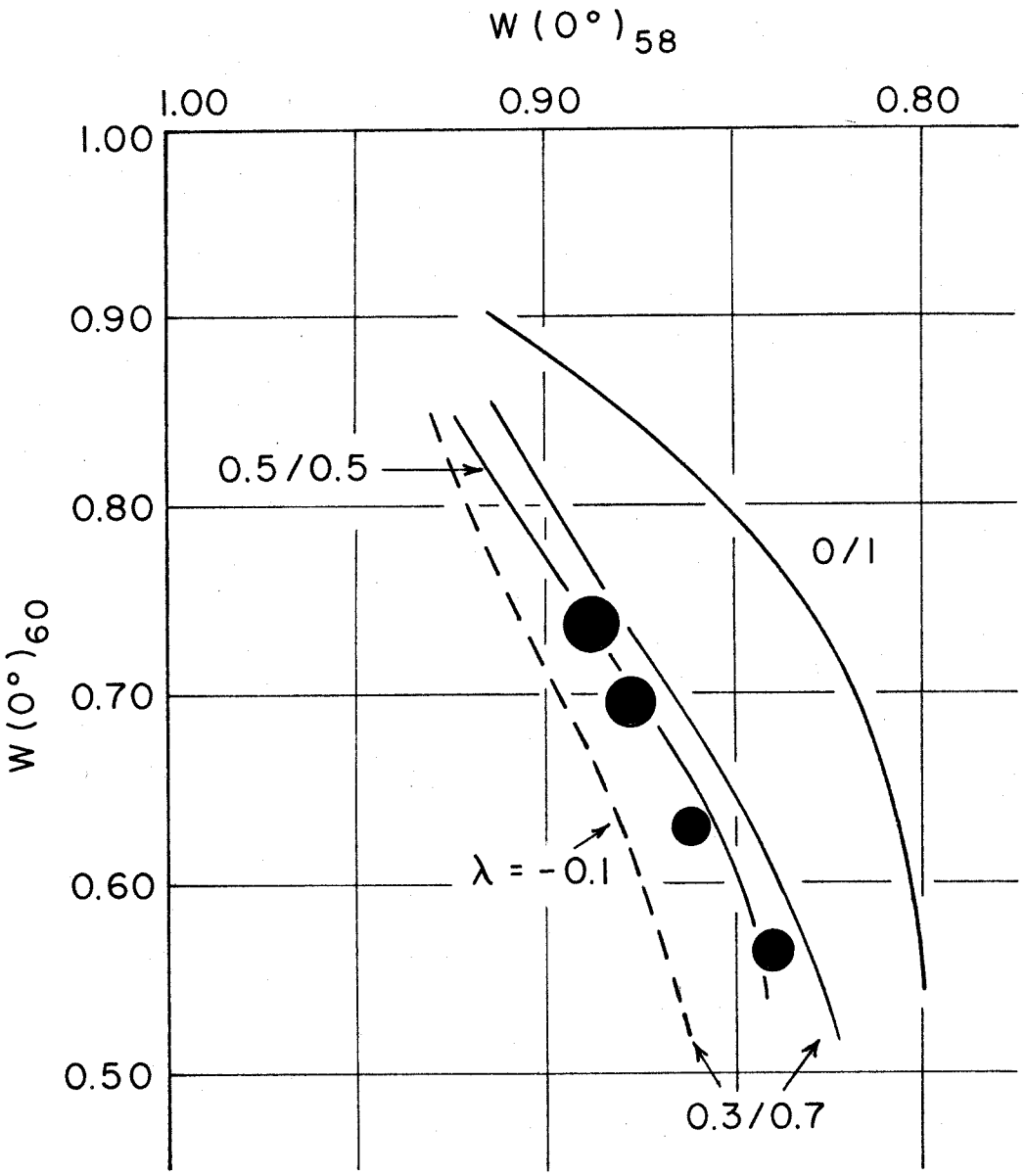

W(0°) FOR Co^{58} VERSUS W(0°) FOR Co^{60} IN $Ce_2Mg_3(NO_3)_{12}\cdot 24H_2O$ WITH A 600 GAUSS EXTERNAL MAGNETIC FIELD ALONG THE SYMMETRY AXIS

Curves are theoretical with three ratios of ionic populations (a_{II}/a_I) in the two different lattice sites. Curves are for $\lambda = 0$ except where noted.

FIGURE 20

REFERENCES

1. P. Debye, Ann. d. Phys. 81, 1154 (1926).
2. W. Giauque, Journ. Am. Chem. Soc. 49, 1864, 1870 (1927).
3. W. de Haas, E. Wiersma, and H. Kramers, Physica 1, 1 (1933-34).
4. W. Giauque and D. MacDougall, Phys. Rev. 43, 768 (1933).
5. N. Kurti and F. Simon, Nature 133, 907 (1934).
6. C. Gorter, Phys. Z. 35, 923 (1934).
7. N. Kurti and F. Simon, Proc. Roy. Soc. London A 149, 152 (1935).
8. C. Gorter, Physica 14, 504 (1948).
9. M. Rose, Phys. Rev. 75, 213 (1949).
10. B. Bleaney, Proc. Phys. Soc. A 64, 315 (1951).
11. J. Daunt, Proc. int. Conf. low temp. Phys. Oxford, (1951), p. 157.
12. C. Gorter, Proc. int. Conf. low temp. Phys. Oxford, (1951), p. 158.
13. M. Grace et al., Comm. Conf. Phys. basses temp. Paris, (1955), p. 263.
14. G. Khutsishvili, J. exp. theor. Phys. USSR, 29, 894 (1955).
15. R. Pound, Phys. Rev. 76, 1410 (1949).
16. C. Gorter, Progress in Low Temperature Physics Vol. II, Interscience Publishers Inc., New York (1957), p. 292.
17. D. Griffing and J. Wheatley, Phys. Rev. 104, 389 (1956).
18. H. Fraunfelder, N. Lavine, A. Rossi, and S. Singer, Phys. Rev. 103, 352 (1956).
19. F. Boehm and A. H. Wapstra, Phys. Rev. 109, 456, (1958).

20. R. Feynman and M. Gell-Mann, Phys. Rev. 109, 193 (1958).

21. K. Bowers and J. Owen, Reports on Progress in Physics XVIII, 304 (1955).

22. B. Bleaney and D. Ingram, Proc. Roy. Soc. A 208, 1943 (1951).

23. H. Tolhoek and J. Cox, Physica XIX, 101 (1953).

24. J. Cox and H. Tolhoek, Physica XIX, 673 (1953).

25. J. Cox, S. deGroot, and C. Hartogh, Physica XIX, 1119 (1953).

26. C. Hartogh, H. Tolhoek, and S. deGroot, Physica XX, 1310 (1954).

27. B. Bleaney and K. Stevens, Reports on Progress in Physics XVI, 108 (1953).

28. P. Dagley, M. Grace, J. Hill, and C. Sowter, Phil. Mag. 3, 489 (1958).

29. N. Kurti, Private Communication to J. Pellam (1957).

30. R. Berman, Advances in Physics 2, 103 (1953).

31. J. Daniels, Can. J. Research 35, 1133 (1957).

32. J. Van Vleck, Electric and Magnetic Susceptibilities, Oxford (1932), Chapt. XII.

33. S. Allison, Phys. Rev. 44, 63 (1933).

34. E. Fermi, Z. Physik 60, 320 (1930).

35. M. Perlman and J. Miskel, Phys. Rev. 91, 899 (1953).

36. D. Strominger, J. Hollander, and G. Seaborg, Revs. Modern Phys. 30, 585 (1958).

37. N. Steenberg, Phys. Rev. 95, 982 (1954).

38. H. Tolhoek, C. Hartogh, and S. deGroot, J. phys. et radium 16, 615 (1955).

39. M. Grace, J. phys. et radium 16, 622 (1955).

40. R. Wyckoff, Crystal Structures, Interscience Publishers Inc., New York (1948), Chapt. X.

41. A. Sommerfield, Thermodynamics and Statistical Mechanics, Academic Press Inc., New York (1956), Sec. 33.

42. C. Garrett, Magnetic Cooling, Harvard University Press, Cambridge, Mass. (1954), p. 21.

43. C. Kittel, Introduction to Solid State Physics, John Wiley & Sons, Inc., New York (1956), p. 591.

44. J. Van Kranendonk and J. Van Vleck, Revs. Modern Phys. 30, 1 (1958).

45. C. Garrett, Magnetic Cooling, Harvard University Press, Cambridge, Mass. (1954), p. 49.

46. W. Dobrov and C. Jeffries, Phys. Rev. 108, 60 (1957).

47. A. Ferguson to W. Sharp, Internal Memo, Chalk River Project.

48. M. Rose, Phys. Rev. 91, 610 (1953).

49. R. Tolman, The Principles of Statistical Mechanics, Oxford University Press (1955), Chapt. IX.

50. J. Dillinger, Low Temperature Physics and Chemistry, University of Wisconsin Press (1958), p. 586.

51. J. Ollom and J. Van Vleck, Physica 17, 205 (1951).